

# Soil Moisture Data Assimilation

Gabriëlle J.M. De Lannoy<sup>1,2</sup>, Patricia de Rosnay<sup>3</sup>, Rolf H. Reichle<sup>1</sup>

*1 NASA Goddard Space Flight Center, Code 610.1, Greenbelt Road, Greenbelt, MD 20771, USA*

*2 Universities Space Research Association, 10211 Wincopin Circle, Columbia, MD 21044*

*3 European Center for Medium-Range Weather Forecasts, Shinfield Park, Reading RG2 9AX, Berkshire, UK*

Gabrielle.DeLannoy@nasa.gov

Patricia.Rosnay@ecmwf.int

Rolf.Reichle@nasa.gov

In Handbook of Hydrometeorological Ensemble Forecasting, edited by Qingyun Duan, Florian Pappenberger, Jutta Thielen, Andy Wood, Hannah Cloke and John C. Schaake.

## Abstract

Accurate knowledge of soil moisture at the continental scale is important for improving predictions of weather, agricultural productivity and natural hazards, but observations of soil moisture at such scales are limited to indirect measurements, either obtained through satellite remote sensing or from meteorological networks. Land surface models simulate soil moisture processes, using observation-based meteorological forcing data, and auxiliary information about soil, terrain and vegetation characteristics. Enhanced estimates of soil moisture and other land surface variables, along with their uncertainty, can be obtained by assimilating observations of soil moisture into land surface models. These assimilation results are of direct relevance for the initialization of hydro-meteorological ensemble forecasting systems. The success of the assimilation depends on the choice of the assimilation technique, the nature of the model and the assimilated observations, and, most importantly, the characterization of model and observation error. Systematic differences between satellite-based microwave observations or satellite-retrieved soil moisture and their simulated counterparts require special attention. Other challenges include inferring root-zone soil moisture information from observations that pertain to a shallow surface soil layer, propagating information to unobserved areas and downscaling of coarse information to finer-scale soil moisture estimates. This chapter summarizes state-of-the-art solutions to these issues with conceptual data assimilation examples, using techniques ranging from simplified optimal interpolation to spatial ensemble Kalman filtering. In addition, operational soil moisture assimilation systems are discussed that support numerical weather prediction at ECMWF and provide value-added soil moisture products for the NASA Soil Moisture Active Passive mission.

1   **Keywords:** Soil moisture retrieval, microwave brightness temperature, radar backscatter,  
2   terrestrial water storage, analysis, innovation, increment, Kalman filter, observation operator,  
3   numerical weather prediction, initialization, state update, calibration, radiative transfer model,  
4   land surface model, screen-level observations, ASCAT, AMSR2, SMOS, SMAP, GRACE

5

6

## 1. Introduction

Soil moisture is the quantity of water contained in the upper layers of the soil, water that directly interacts with the atmosphere through evapotranspiration and partitions rainfall into infiltration and runoff. While the exact definition of soil moisture is slightly different for weather forecasters, farmers, water managers, construction engineers, and ecologists, in hydrological and Earth system applications, soil moisture usually includes the water in the upper ~1-2 m of the soil. Even though soil moisture represents only 0.0012% of all water available on Earth (~ 1.4 billion km<sup>3</sup>), and only 0.05% of all fresh water (~ 35,000 km<sup>3</sup>) (Gleick, 1996), it is of primary importance because it links the water, energy and carbon cycles and therefore has a significant impact on weather and global climate (Dirmeyer, 2000, Koster *et al.*, 2004), and it controls droughts and floods, agricultural yield, diseases, and other socio-economic phenomena.

Soil moisture is being monitored with modeling and observing systems. Numerical models provide spatially and temporally continuous estimates of soil moisture at customized space and time resolutions, and at various soil depths down to the water table. However, models are always simplified and prone to errors. Observations are usually obtained from sparse in situ networks or satellite swaths and they are therefore limited in their spatial and temporal coverage. One particularly important limitation of current remote sensing observations is that they only provide soil moisture in a shallow surface layer. By using models and observations synergistically, observational gaps can be filled and superior estimates of soil moisture can be constructed. This process, known as data assimilation, merges the observations into soil moisture modeling systems, either to improve model simulations or to add value to observations.

1

2 The focus of this chapter is on updating the soil moisture state in dynamic land surface models for  
3 continental and global applications. At these scales, observations related to soil moisture are  
4 mainly provided by global surface observational networks or through remote sensing, either in the  
5 form of satellite retrievals, microwave radiances or radar backscatter values. Data assimilation  
6 interpolates and extrapolates the observations in space and time and updates the entire simulated  
7 soil moisture column, while ensuring consistency with all other geophysical variables in the model.  
8 This process leads to improved initial conditions for subsequent hydro-meteorological forecasts  
9 across a range of applications such as weather and drought forecasts. In addition, meaningful  
10 estimates of the uncertainty in soil moisture estimates can be obtained, provided the characteristics  
11 of observation and forecast error are well described in the assimilation system. These uncertainty  
12 estimates can be used to quantify the uncertainty in hydro-meteorological ensemble forecasts  
13 (Chapter X404, 639X).

14

15 A broader definition of ‘data assimilation’ methods aimed at improving soil moisture estimates  
16 might include the construction of improved forcing information, the revision of modeling systems,  
17 or the estimation of model parameters (Chapter X628X and X629X) using in situ or satellite  
18 observations. Parameter estimation is crucial to limit biases in the modeling part of the  
19 assimilation system. This mostly involves the calibration of static model parameters against  
20 historical data sets. The dynamic estimation of evolving parameters, possibly along with soil  
21 moisture updates, has also been explored, but not for large-scale soil moisture modeling systems.  
22 The use of observational information to construct superior forcing information and improve

modeling systems is at the core of land surface re-analysis products generated by various operational groups (section 9).

The objective of this chapter is to educate students and scientists new to the discipline about the current, well established, practices in large-scale soil moisture data assimilation, without providing an in depth literature review. The chapter first provides an overview of the components of a soil moisture data assimilation system (section 2). Next, the assimilated observations (section 3), the soil moisture modeling (section 4) and the modeling of observation predictions (section 5) are discussed. State-of-the-art assimilation techniques for soil moisture state updating are presented in section 6, with attention to an optimal characterization of random and systematic errors (section 7). The implementation of advanced ensemble Kalman filter systems is highlighted for its direct relevance to hydro-meteorological ensemble forecasting. Section 8 discusses the evaluation of large-scale assimilation results with in situ soil moisture observations. Section 9 provides examples of cutting-edge, pre-operational soil moisture assimilation systems. The chapter is concluded with a summary (section 10).

## **2. Components of a Soil Moisture Data Assimilation System**

The basic components of a data assimilation system include observations (section 3), modeling (section 4 and 5), and the analysis update (section 6). The observations used for large-scale soil moisture data assimilation systems include screen-level observations or remote sensing observations. The modeling comprises two parts: (i) the prognostic land surface model to

dynamically propagate the state and (ii) diagnostic modeling to translate land surface variables (for example, soil moisture) into observed quantities such as remotely sensed radiances. The analysis update optimally combines the information from the observations and the model.

The land surface system (section 4) dynamically propagates the prognostic land surface variables in time. The prognostic variables are the key variables that are needed to initialize or restart a model simulation. Depending on the formulation of the land surface model, the prognostic variables could consist of soil moisture, soil temperature and snow in all its layers, as well as vegetation variables. These model variables have a memory of the past and evolve in time governed by physical laws such as energy and mass conservation and gravity, and in response to external meteorological forcings, such as precipitation and evapotranspiration. The land surface model  $\mathbf{f}_{i,i-1}(\cdot)$  uses the estimate of the state  $\hat{\mathbf{x}}_{i-1}^+$  at the previous time  $i-1$  (which is an *a posteriori* or *analysis* estimate, if observations were used to update it, see section 6) together with external forcings information  $\mathbf{u}_i$  to predict the state  $\hat{\mathbf{x}}_i^-$  at the current time  $i$ , also called the *a priori* or *forecast* state estimate. For simplicity, the land surface parameters  $\boldsymbol{\alpha}$  are assumed constant. The state trajectory can be written as:

$$\hat{\mathbf{x}}_i^- = \mathbf{f}_{i,i-1}(\hat{\mathbf{x}}_{i-1}^+, \mathbf{u}_i, \boldsymbol{\alpha}) \quad (1)$$

which approximates the true system:

$$\mathbf{x}_i = \mathbf{f}_{i,i-1}(\mathbf{x}_{i-1}, \mathbf{u}_i, \boldsymbol{\alpha}, \mathbf{w}_i) \quad (2)$$

where model errors  $\mathbf{w}_i$  are due to errors in the external forcings  $\mathbf{u}_i$ , in the model  $\mathbf{f}_{i,i-1}(\cdot)$  structure and parameters  $\boldsymbol{\alpha}$ . Errors in the analysis state  $\hat{\mathbf{x}}_{i-1}^+$  and model errors  $\mathbf{w}_i$  will introduce errors in the forecasted state  $\hat{\mathbf{x}}_i^-$ . The uncertainties in  $\hat{\mathbf{x}}_{i-1}^+$ ,  $\mathbf{w}_i$  and  $\hat{\mathbf{x}}_i^-$  are described by the analysis error

covariance  $\mathbf{P}_{i-1}^+$ , the model error covariance  $\mathbf{Q}_i$  and the forecast error covariance matrix  $\mathbf{P}_i^-$ , respectively. One way to estimate the uncertainties is to generate an ensemble of trajectories  $\hat{\mathbf{x}}_{i,j}^-$  by perturbing forcings, state variables or parameters (further discussed in section 7.2.1).

The surface soil moisture that is simulated with a land surface model is often directly comparable to satellite-based soil moisture retrievals. If the land surface model output does not directly correspond to the assimilated observations, such as for brightness temperature or radar backscatter observations, a second modeling step is needed to transform the land model output into observation predictions  $\hat{\mathbf{y}}_i^-$  (section 5):

$$\hat{\mathbf{y}}_i^- = \mathbf{h}_i(\hat{\mathbf{x}}_i^-, \boldsymbol{\beta}) \quad (3)$$

This observation model, or *observation operator*,  $\mathbf{h}_i(\cdot)$  maps state variables from state space to observation space. This step may also include any spatial or temporal aggregation of land surface variables to satellite-scale observation predictions. Here again, for simplicity, the parameters  $\boldsymbol{\beta}$  of the observation operator are assumed constant and uncertainties in the observation predictions could be estimated through ensemble methods.

The assimilated observations  $\mathbf{y}_{\text{obs},i}$  (section 3) can be written as function of the true state  $\mathbf{x}_i$  and the observation operator  $\mathbf{h}_i(\cdot)$ :

$$\mathbf{y}_{\text{obs},i} = \mathbf{h}_i(\mathbf{x}_i, \boldsymbol{\beta}, \mathbf{v}_i) \quad (4)$$



1 The observation error term  $\mathbf{v}_i$  includes measurement errors as well as representativeness errors and  
2 is assumed additive in most data assimilation systems. The corresponding observation error  
3 covariance matrix will be denoted as  $\mathbf{R}_i$  (discussed in section 7.2.2).

4  
5 The difference between the observations and observation predictions is used to update the state in  
6 the analysis step (section 6), for example as follows:

$$\hat{\mathbf{x}}_i^+ = \hat{\mathbf{x}}_i^- + \mathbf{K}_i[\mathbf{y}_{\text{obs},i} - \hat{\mathbf{y}}_i^-] \quad (5)$$

7 where  $\mathbf{K}_i$  is a gain matrix. In most soil moisture data assimilation systems, the state  $\hat{\mathbf{x}}_i^-$  used in the  
8 updating procedure is a limited subset of the land model prognostic variables that renders the  
9 system ‘observable’. (For simplicity, the same notation  $\hat{\mathbf{x}}_i^-$  is used for either the full set or a subset  
10 of prognostic variables.) A system is observable if the state  $\hat{\mathbf{x}}_i^-$  is sufficiently connected to the  
11 assimilated observations  $\mathbf{y}_{\text{obs}}$ . In practice, the state in Eq. (5) contains ‘observed’ state variables  
12 that directly contribute to observation predictions, plus ‘unobserved’ variables that are correlated  
13 (in the errors) to the ‘observed’ state variables and that will be updated along with the observed  
14 state variables during the data assimilation. For example, for the assimilation of surface soil  
15 moisture retrievals, the state vector will contain both (observed) surface and (unobserved) deeper  
16 layer soil moisture (section 6.1). Furthermore, the state vector can contain state variables for  
17 multiple fine-scale grid cells needed to generate coarser-scale observation predictions,  
18 ‘unobserved’ neighboring grid cells (section 6.1.4), and state variables at different time steps  
19 (section 6.2).

### 3. Observations Related to Soil Moisture

Global-scale soil moisture can be inferred from global surface observational networks or from satellite-based observations. Near-surface meteorological observations of two meter air temperature and relative humidity are measured routinely by the land surface synoptic report (SYNOP) operational network at the global scale and, under certain conditions, are related to surface and root zone soil moisture. The coverage of these station observations varies greatly between dense measurements in Europe, North America and parts of Asia and significantly sparser coverage elsewhere. Screen-level variables are assimilated operationally at major numerical weather prediction centers because their assimilation improves medium-range forecasts of surface meteorological conditions, albeit with limited improvement to the soil moisture estimates themselves (section 6.1.1).

Satellite remote sensing offers a way to observe the surface soil water content at continental to global scales. Most existing remote sensing devices use the distinct physical properties of soil water in interaction with electromagnetic signals at specific wavelengths. Microwave radiometry (wavelength 1-20 cm, frequency 10-1.4 GHz) has been used for several decades to estimate the soil's dielectric constant, and hence soil moisture. Examples of radiometers onboard satellite platforms that passively measure microwave emission from the land surface are the Advanced Microwave Sounding Radiometer 2 (AMS2), the Microwave Imaging Radiometer using Aperture Synthesis onboard the Soil Moisture Ocean Salinity (SMOS) mission, the Aquarius radiometer, and the radiometer onboard the Soil Moisture Active Passive (SMAP) mission, among others. Active microwave sensors send and receive microwave signals. Examples include the

radars onboard the two European Remote Sensing satellites (ERS-1 and ERS-2), the Advanced SCATterometer (ASCAT) onboard the European Organisation for the Exploitation of Meteorological Satellites (METOP) series of satellites and also the radar onboard SMAP. All the above mentioned satellites are polar orbiting, and each provides global coverage approximately every 2 to 3 days.

Microwave remote sensing is attractive because the signals at L-band wavelengths (1.4 GHz) used for SMOS and SMAP are most sensitive to soil moisture, less impacted by vegetation, and not impacted by clouds or light rain. There are, however, some obvious limitations: (i) microwave instruments only sense the soil moisture in a thin (1-5 cm) surface layer, with the penetration depth depending on the microwave wavelength and soil moisture content, (ii) the spatial coverage is limited to swaths of ~250–1000 km and the revisit time is once every couple of days, (iii) passive microwave data have coarse spatial resolutions (~10-100 km), and (iv) active microwave data are typically very noisy. Through data assimilation, some of these limitations can be overcome, as will be illustrated in section 6.

Microwave observations can be assimilated directly as brightness temperatures or backscatter values or after inversion to soil moisture retrievals. Various methods exist to infer soil moisture retrievals from active or passive microwave signals. For example, AMSR2, SMOS and SMAP retrievals are obtained by explicitly inverting the relationship between soil moisture and passive microwave emission (e.g. *Wigneron et al., 2007*) and ASCAT retrievals employ a change detection

1 technique (e.g. *Bartalis et al., 2007*). It is important to note that the climatologies of various  
2 retrieval products can be very different and require careful attention when comparing or merging  
3 various retrieval products (*Dorigo et al., 2015, Reichle and Koster, 2004*). The soil moisture  
4 retrieval process is very sensitive to radiative transfer or backscatter model parameters (section  
5 5.2), and to auxiliary information (e.g. about soil temperature and vegetation) provided by land  
6 surface modeling systems. For example, the SMOS soil moisture retrievals use ECMWF's  
7 simulated surface soil temperature and moisture as prior information in the retrieval and SMAP  
8 retrievals use prior and auxiliary information from the NASA Goddard Earth Observing System  
9 Model, version 5 (GEOS-5) (section 4). In addition, retrievals can technically be calculated under  
10 any conditions, but the soil moisture estimates are only meaningful in areas with moderate  
11 topographic complexity, non-frozen and snow-free conditions, sparse vegetation and at times with  
12 limited precipitation.

13  
14 An alternative to using microwave signals is to use gravity measurements to determine changes in  
15 the mass of water: the Gravity Recovery and Climate Experiment (GRACE) mission consists of  
16 two satellites whose relative distance and velocity can be related to anomalies in water amounts at  
17 and near the land surface, including soil moisture, snow, and surface water. GRACE observations  
18 thus provide information on deeper soil moisture under any weather conditions, but their resolution  
19 is very coarse in space (~250 km) and time (monthly).

#### 4. Land Surface Modeling

A wide variety of models has been used to simulate the dynamic evolution of soil moisture, ranging from simple solutions of equations that represent the movement of water in unsaturated soils to full land surface models (LSM, [Chapter X626X](#)) that simulate the soil-vegetation-atmosphere interactions. The strength of models is in their reliance on physical laws known to operate in nature and in their ability to provide a consistent and balanced distribution of water and heat. Historically, some LSMs have been optimized to simulate select land surface variables for specific regions, whereas others are tuned to provide good boundary information in general circulation models, sometimes with little attention paid to the physical realism of the simulated soil moisture. Examples of LSMs that are part of operational integrated modeling systems are the Hydrology-Tiled ECMWF Scheme for Surface Exchanges over Land (HTESSEL, *Balsamo et al., 2009*) in ECMWF's operational Integrated Forecasting System (IFS) and the Catchment land surface model (*Koster et al., 2000*) in NASA's GEOS-5 system.

The prognostic variables related to soil moisture (i.e. part of  $\hat{\mathbf{x}}_i^-$  in Eq. 1) are very different in these models. In HTESSEL the soil moisture is calculated in four layers of thicknesses of 0.07, 0.21, 0.72 and 1.89 m from top to bottom. The Catchment model defines three prognostic variables that describe the equilibrium soil moisture profile and deviations from the equilibrium across the entire watershed (or modeling unit). Specifically, the catchment deficit (catdef), root-zone excess (rzexc), and surface excess (srfexc) prognostic variables are used together to diagnose soil moisture in a surface layer (sfmc, 0-0.05 m), a root-zone layer (rzmc, 0-1 m) and the entire profile (prmc). The latter extends from the surface to the bedrock at a variable depth between 1.3 and 10

m. The temperature ( $t_{\text{soil}}$ ) of the topmost soil layer (of thickness 0.1 m) is diagnosed from the corresponding ground heat content prognostic variable ( $ght$ ).

The LSM structure (denoted  $\mathbf{f}_{i,i-1}(\cdot)$  in Section 2), parameters ( $\alpha$ ), and forcing inputs ( $\mathbf{u}_i$ ) determine the climatology of the simulated soil moisture, that is, its long-term average and seasonal variation. For example, the porosity parameter determines the maximum amount of water that can be contained in a soil layer and the hydraulic conductivity determines how fast soil moisture moves across soil layers. Locally optimal parameters for soil moisture modeling could be found through calibration against historic data records of observations (Chapter X628X). However, the calibration of LSMs is a non-trivial task, because of multi-parameter interactions, equifinality and the scale-dependency of the land model parameters. Global LSMs are usually not calibrated and solely rely on auxiliary static information about soil and vegetation properties. Soil physical parameters, for example, are typically inferred from global soil texture maps using static look-up tables or pedotransfer functions. These parameters are not perfect, yet they determine the average (climatological) level of soil moisture and may thus be responsible for persistent biases. LSM parameters also impact random errors because they affect the nature of shorter-term soil moisture dynamics.

The most important forcing input to soil moisture simulations is precipitation, but other surface meteorological fields are also required, including radiation, air temperature and humidity, and wind speed. For small-scale applications, forcing data are usually collected from meteorological

towers. Forcing data for large-scale applications rely on a merger of surface observations and atmospheric re-analysis fields. Examples include the recent MERRA-Land (*Reichle et al., 2011*) and ERA-Land (*Balsamo et al., 2013*) products. The underlying atmospheric reanalysis products assimilate a very large number of conventional and satellite-based observations of the atmosphere into a global atmospheric model and provide self-consistent meteorological fields with complete spatial and temporal coverage. However, these products have a relatively coarse resolution and are subject to errors in the re-analysis systems. Errors in the long-term average precipitation amounts or intensity result in biased simulations. At shorter time scales, missed or excessive precipitation events cause random errors in simulated soil moisture. Merging the reanalysis data with satellite and gauge-based precipitation data products mitigates some, but not all, of these errors.

Another determining factor for soil moisture simulations is the land model initialization. A so-called “cold” model start (using an arbitrary state initialization) will generally cause a drift in soil moisture until a steady soil moisture level is reached, which typically takes simulations across several years. It is therefore important to spin up the model until its prognostics are in agreement with the climatological boundaries as determined by the forcings and model parameters.

## **5. Observation Operator**

If satellite-based soil moisture retrievals are assimilated, then the model output from land surface models can be directly compared to the assimilated observations. However, the assimilation of

screen-level observations, microwave observations and terrestrial water storage anomalies requires a diagnostic modeling step with an observation operator that facilitates the direct comparison between the land model output and the observed variables (*Reichle et al., 2014*).

### 5.1. Screen-Level Observation Predictions

Screen-level observations are in situ measurements of temperature and relative humidity ( $T_{2m,obs}$ ,  $RH_{2m,obs}$ ) at 2 m above the land surface. In global atmospheric models, estimates of  $\widehat{T}_{2m}^-$  and  $\widehat{RH}_{2m}^-$  are typically obtained by interpolating the model variables from the surface (as computed by the land surface model component) to the atmospheric conditions at the height of lowest atmospheric model level (*Mahfouf et al., 2009*), following the Monin-Obukhov similarity theory. The latter describes flow and turbulence properties in the lowest 10% of the atmospheric boundary layer. This assumes that the first atmospheric level is not at 2 m, but instead imposed higher up. Formally, this can be written as:

$$\begin{bmatrix} \widehat{T}_{2m}^- \\ \widehat{RH}_{2m}^- \end{bmatrix} = \mathbf{h}_{2m}(\widehat{\mathbf{x}}^-, \mathbf{u}, \boldsymbol{\beta}_{2m}) \quad (6)$$

where  $\widehat{\mathbf{x}}^- = [\widehat{sfmc}^-, \widehat{rzm}^-, \widehat{tsurf}^-, \widehat{tsoil}^-]^T$  are the land surface state variables, including surface and root-zone soil moisture, and surface and soil temperature, respectively. The vector  $\mathbf{u}$  contains the imposed atmospheric variables, with air temperature, humidity and wind speed at the lowest atmospheric level, and  $\mathbf{h}_{2m}(\cdot)$  represents the vertical interpolation with  $\boldsymbol{\beta}_{2m}$  the interpolation parameters.



## 5.2. Microwave Observation Predictions

Passive microwave emission from the land surface is often referred to as brightness temperature ( $T_b$ ) and measured for certain polarizations, wavelengths and incidence angles, collectively denoted as the instrument configuration. The brightness temperature for a given configuration ( $c$ ) can be simulated as a function of surface soil temperature, attenuated by soil and vegetation characteristics:

$$\widehat{Tb}_c^- = \mathbf{h}_p(\widehat{\mathbf{x}}^-, \boldsymbol{\beta}_p, \mathbf{c}_p) \quad (7)$$

with  $\mathbf{h}_p(.)$  a radiative transfer model for passive (p) microwave emission,  $\widehat{\mathbf{x}}^- = [\widehat{sfmc}^-, \widehat{tsurf}^-, \widehat{tsoil}^-]^T$  a set of dynamic land surface variables such as surface soil moisture, and surface and soil temperature,  $\boldsymbol{\beta}_p$  a vector with land surface specific parameters, including the microwave soil roughness length, scattering albedo, vegetation parameters, and  $\mathbf{c}_p$  a set of radiometer configuration constants.

Active radar backscattering coefficients ( $\sigma^0$ ) measured for a given sensor configuration  $c$  can be similarly related to land surface variables as follows:

$$\widehat{\sigma}_c^{0-} = \mathbf{h}_a(\widehat{\mathbf{x}}^-, \boldsymbol{\beta}_a, \mathbf{c}_a) \quad (8)$$

with  $\mathbf{h}_a(.)$  the backscattering model for active (a) microwave signals,  $\widehat{\mathbf{x}}^-$  again a set of dynamic land surface variables including soil moisture,  $\boldsymbol{\beta}_a$  a vector with land surface specific parameters, such as the root mean square (rms) surface height and correlation length to quantify the roughness and  $\mathbf{c}_a$  a set of radar properties.

1

2 Figure 1 illustrates the non-linear relationship between the surface soil moisture content sfmc and  
3  $Tb_c$  or  $\sigma_c^0$  as simulated by physically-based radiative transfer and backscattering models over bare  
4 soil. In these models, soil moisture is first converted to a soil dielectric constant using a dielectric  
5 mixing model. The dielectric constant then determines the surface reflectivity and thus the  
6 emission, reflection and scattering of waves. Figures 1a-b use a zero-order radiative transfer model  
7 (*Mo et al., 1982*) as  $h_p(.)$  for  $Tb_c$  simulation. Figures 1c-d use the Integral Equation Model (*Fung*  
8 *et al. 1992*) as  $h_a(.)$  for  $\sigma_c^0$  simulation. For the illustrations in the figure the sensor configurations  $c$   
9 are chosen according to the design of the radiometer and radar sensors onboard SMAP, i.e. with  
10 an incidence angle of  $40^\circ$ , either horizontal (H) or vertical (V) polarization (co-polarization for the  
11 radar), and a frequency of 1.41 GHz for the radiometer and 1.26 GHz for the radar. Figures 1a-b  
12 illustrate that the brightness temperature is close to surface soil temperature ( $T_s$ ) under dry  
13 conditions and it decreases with soil moisture. As a rule of thumb, a 2–3 K increase in  $Tb$  is  
14 associated with a  $0.01 \text{ m}^3/\text{m}^3$  decrease in soil moisture for incidence angles around  $40^\circ$  and for low  
15 vegetation regions (vegetation water content of less than about  $5 \text{ kg}/\text{m}^2$ ). Figures 1c-d show that a  
16 1-5 dB decrease in  $\sigma_c^0$  can be expected for a  $0.1 \text{ m}^3/\text{m}^3$  decrease in soil moisture below  $0.35 \text{ m}^3/\text{m}^3$ ,  
17 whereas little sensitivity is found for wetter soil moisture. The figure further highlights the  
18 sensitivity of the relationships to a change in only one select parameter ( $\in \beta$ ), i.e. the microwave  
19 roughness  $HR$  [-] for  $Tb_c$  simulation or the rms surface height [cm] for  $\sigma_c^0$  simulation. A realistic  
20 range of  $h$  (Figure 1a-b) easily introduces differences of 50 K or more in  $Tb$  for a moderate level  
21 of soil moisture. Figure 1c-d show that a 1 cm increase in the rms roughness parameter could  
22 increase the backscattering by 5 dB. In reality, vegetation further complicates the picture. To

summarize, the relationship between the soil moisture content and  $Tb_c$  or  $\sigma_c^0$  is highly dependent on a set of very uncertain parameters.

### 5.3 Terrestrial Water Storage Predictions

Changes in terrestrial water storage (TWS) are among the dominant mass variations that can be detected in the GRACE signal (Rodell *et al.*, 2007). The simulated monthly TWS represents the vertically integrated water amount as:

$$\widehat{TWS}^- = \mathbf{h}_{TWS}(\hat{\mathbf{x}}^-, \boldsymbol{\beta}_{TWS}) \quad (9)$$

with  $\mathbf{h}_{TWS}(\cdot)$  the vertical integration of the individual components of  $\hat{\mathbf{x}}^- = [\widehat{sfmc}^-, \widehat{rzmc}^-, \widehat{gwt}^-, \widehat{snow}^-, \widehat{ice}^-, \dots]^T$ , including surface soil moisture, root-zone soil moisture, depth to the ground water table (gwt), snow, ice and possibly water stored in or on vegetation, and  $\boldsymbol{\beta}_{TWS}$  refers to any parameters needed to compute the TWS. The corresponding observations are mostly provided in terms of anomalies, i.e. as deviations from a long-term (multi-month, multi-year) average, which is not necessarily known. For assimilation into a model, the observed TWS anomalies are typically converted to actual  $TWS_{obs}$  by adding a long-term model estimate  $\langle \widehat{TWS}^- \rangle$ .

## 6. Assimilation of Observations Related to Soil Moisture

### 6.1 Sequential State Updating

Popular methods for the sequential assimilation of soil moisture observations at large scales include direct insertion, nudging and statistical correction (Dharssi *et al.*, 2011), optimal interpolation (Mahfouf *et al.*, 2009), Extended Kalman filtering (Sabater *et al.*, 2007), variational

assimilation (Reichle et al., 2001, Hess et al., 2008), ensemble Kalman filtering (Reichle et al., 2002) and particle filtering (Pan et al., 2008). Details of these techniques are given in Chapter X632X. The ensemble Kalman filter and particle filtering variants are the methods that lend themselves most directly to integration in hydro-meteorological ensemble forecast systems.

Sequential filtering involves cycling through two steps, as summarized in Table 1. In the first step, a *background, a priori* or *forecast state* estimate is generated with a dynamic model  $\mathbf{f}_{i,i-1}(\cdot)$ . This forecast could either be deterministic, i.e.  $\hat{\mathbf{x}}_i^-$ , or consist of an ensemble  $\hat{\mathbf{x}}_{i,j}^-$  where forecast perturbations ( $\mathbf{w}_{i,j}$ ) are applied to generate each ensemble member  $j$  ( $j=1,\dots,N$ ). The second step generates an *a posteriori* or *analysis* state by correcting the state with observations, as in Eq. (5). Two update variants have been classic for the assimilation of soil moisture observations. The most commonly used variant adds an *increment* to the forecasted state. This increment is determined using the difference between observations and observation predictions  $[\mathbf{y}_{\text{obs},i} - \hat{\mathbf{y}}_i^-]$  and a blending matrix, or gain matrix  $\mathbf{K}_i$ . In ‘optimal’ (minimum analysis error variance) assimilation schemes, the gain  $\mathbf{K}_i$  is found by weighting the uncertainty in the forecast state  $\mathbf{P}_i^-$  and in the observations  $\mathbf{R}_i$ . If the forecast error covariance  $\mathbf{P}_i^-$  is dynamically propagated in time, then  $\mathbf{K}_i$  is called a Kalman gain. If  $\mathbf{P}_i^-$  is diagnosed from ensemble forecasts, then the filter is called an ensemble Kalman filter. Another update variant preferentially weighs a set of possible forecasts (particles, ensemble members) so that the resulting observation prediction is closest to observations. This approach is used in particle filters, which have a great potential for soil moisture assimilation problems and subsequent ensemble forecasting, but have not yet been explored thoroughly for large-scale or multi-scale land surface data assimilation.

1

2 The following examples conceptually describe the assimilation of various soil moisture  
 3 observations using filtering techniques with increasing complexity. Each example can be seen as  
 4 a variant of the basic sequential update Equation (5). It is important to note that the combinations  
 5 of the selected observation types and assimilation techniques are not exclusive and only chosen  
 6 for illustrative purposes.

7

### 8 6.1.1 Screen-Level Data Assimilation Illustrated with Optimal Interpolation

9 Screen-level observations ( $T_{2m,obs}$ ,  $RH_{2m,obs}$ ) have been assimilated operationally for numerical  
 10 weather prediction (NWP) (*Giard and Bazile 2000, Bélair et al., 2003*). To limit the computational  
 11 effort, the state vector is often limited to a few prognostic variables. Consider a state consisting of  
 12 surface moisture content (sfmc), root-zone soil moisture (rzmc), surface temperature (tsurf) and  
 13 soil temperature (tsoil). The typical update equation can be written as:

$$14 \quad \begin{bmatrix} \widehat{sfmc} \\ rzmc \\ tsurf \\ tsoil \end{bmatrix}_i^+ = \begin{bmatrix} \widehat{sfmc} \\ rzmc \\ tsurf \\ tsoil \end{bmatrix}_i^- + \mathbf{K}_i \left( \begin{bmatrix} T_{2m} \\ RH_{2m} \end{bmatrix}_{obs} - \begin{bmatrix} \widehat{T}_{2m} \\ \widehat{RH}_{2m} \end{bmatrix}_i^- \right) \quad (10)$$

15 The initial implementations of this analysis scheme at operational centers use a priori defined  
 16 constants for the  $\mathbf{K}_i$  matrix (4x4). These constants are a priori calibrated, do not use any explicit  
 17 observation operator or any statistical information about background or observation errors.  
 18 Theoretically this approach cannot be classified as “optimal interpolation”, but it has been  
 19 commonly referred to as such in the literature.

Optimal interpolation uses explicit expressions for the a priori and observation error covariance matrices to determine the  $\mathbf{K}_i$  matrix. At Météo-France and at ECMWF the blending matrix  $\mathbf{K}_i$  for the assimilation of screen-level observations uses statistical error information and is further advanced by the use of analytical Jacobians of the land surface model (*Mahfouf et al., 2009, Drusch et al., 2009, de Rosnay et al., 2013*), i.e.:

$$\mathbf{K}_i = \mathbf{B}\mathbf{H}_i^T [\mathbf{H}_i\mathbf{B}\mathbf{H}_i^T + \mathbf{R}]^{-1} \quad (11)$$

with  $\mathbf{B}$  (4x4) a time-invariant background error covariance matrix,  $\mathbf{R}$  (2x2) a time-invariant diagonal observation error covariance matrix and  $\mathbf{H}_i = \left. \frac{\partial \mathbf{h}}{\partial \mathbf{x}} \right|_{\hat{\mathbf{x}}_i^-}$  the linearized observation operator of dimension (2x4). The observation operator  $\mathbf{h}_i(\cdot)$  is a physically-based model and the Jacobian elements are computed in finite differences, i.e. the change in  $\hat{\mathbf{T}}_{2m}^-$  and  $\widehat{\mathbf{RH}}_{2m}^-$  is computed for a small perturbation in the individual state components (sfmc, rzmc,...). The  $\mathbf{H}_i$  matrix maps differences between simulated and observed screen-level variables (*innovations*) to updates (*increments*) in soil moisture and temperature. In general, the limited sensitivity of  $\hat{\mathbf{T}}_{2m}^-$  or  $\widehat{\mathbf{RH}}_{2m}^-$  to root-zone soil moisture leads to small updates (*Drusch et al., 2009*).

The above approach of using a dynamic Jacobian for the observation operator in the blending matrix  $\mathbf{K}_i$  has been referred to as “simplified Extended Kalman filtering” by the land surface community involved in NWP, because of its close ties with the Extended Kalman filter. However,

the use of a fixed background error covariance matrix by definition means that no Kalman filtering is involved, and the assimilation technique is theoretically an ‘optimal interpolation’.

#### 6.1.2 Soil Moisture (Retrieval) Data Assimilation Illustrated with (Extended) Kalman Filtering

The (Extended) Kalman filter (EKF) is similar to the optimal interpolation method in its incremental update equation. The difference is that the Kalman filter dynamically propagates the a priori error covariance matrix, using a linear dynamic model. The (E)KF or its close variants (*Sabater et al., 2007, Hess et al., 2008*) have not been widely used for operational soil moisture data assimilation, because land surface models typically require a rather complex linearization. However, the (E)KF provides the fundamentals to all other Kalman filter variants.

Assume that observations (e.g. retrievals) of soil moisture content ( $\text{sfmc}_{\text{obs}}$ ) are assimilated into a model, with surface and root-zone soil moisture as the state variables. The update equation is:

$$\begin{bmatrix} \widehat{\text{sfmc}} \\ \widehat{\text{rzmc}} \end{bmatrix}_i^+ = \begin{bmatrix} \widehat{\text{sfmc}} \\ \widehat{\text{rzmc}} \end{bmatrix}_i^- + \mathbf{K}_i [\text{sfmc}_{\text{obs}} - \widehat{\text{sfmc}}^-]_i, \text{ with} \quad (12)$$

$$\mathbf{K}_i = \mathbf{P}_i^- \mathbf{H}_i^T [\mathbf{H} \mathbf{P}_i^- \mathbf{H}^T + \mathbf{R}]_i^{-1} = \begin{bmatrix} \sigma_{\widehat{\text{sfmc}}}^2 \\ \rho \cdot \sigma_{\widehat{\text{sfmc}}}^- \cdot \sigma_{\widehat{\text{rzmc}}}^- \end{bmatrix}_i [\sigma_{\widehat{\text{sfmc}}}^2 + \sigma_{\text{sfmc,obs}}^2]_i^{-1} \quad (13)$$

$$\mathbf{P}_i^+ = [\mathbf{I} - \mathbf{K} \mathbf{H}]_i \mathbf{P}_i^- \quad (14)$$

where  $\mathbf{H} = [1 \ 0]$  in this case, but the linearized observation operator could be written more generally as  $\mathbf{H}_i = \left. \frac{\partial \mathbf{h}}{\partial \mathbf{x}} \right|_{\hat{\mathbf{x}}_i^-}$ . The observation error variance is  $\sigma_{\text{sfmc,obs},i}^2$ , the observation prediction error

1 variance is  $\sigma_{\widehat{\text{sfmc}}_i}^2$  and  $\mathbf{P}_i^-$  (2x2) contains a time-variable priori surface and root-zone error variances  
 2  $(\sigma_{\widehat{\text{sfmc}}_i}^2, \sigma_{\widehat{\text{rzmc}}_i}^2)$  on the diagonal, and covariances  $\rho_i \cdot \sigma_{\widehat{\text{sfmc}}_i} \cdot \sigma_{\widehat{\text{rzmc}}_i}$  as off-diagonal elements:

$$3 \quad \mathbf{P}_i^- = \begin{bmatrix} \sigma_{\widehat{\text{sfmc}}_i}^2 & \rho_i \cdot \sigma_{\widehat{\text{sfmc}}_i} \cdot \sigma_{\widehat{\text{rzmc}}_i} \\ \rho_i \cdot \sigma_{\widehat{\text{sfmc}}_i} \cdot \sigma_{\widehat{\text{rzmc}}_i} & \sigma_{\widehat{\text{rzmc}}_i}^2 \end{bmatrix}_i \quad (15)$$

4 It is through the error correlations ( $\rho_i$ ) in  $\mathbf{P}_i^-$  that surface soil moisture *innovations*  $[\text{sfmc}_{\text{obs}} - \widehat{\text{sfmc}}^-]_i$   
 5  $[\text{sfmc}_{\text{obs}} - \widehat{\text{sfmc}}^-]_i$  are propagated to both surface and root-zone *increments*  $\mathbf{K}_i[\text{sfmc}_{\text{obs}} - \widehat{\text{sfmc}}^-]_i$ . The a priori  
 6  $\mathbf{P}_i^-$  is reduced to  $\mathbf{P}_i^+$  after each assimilation update (Eq. 14).

7

8 The a priori  $\mathbf{P}_i^-$  is determined dynamically as function of the modeling system. For additive  
 9 Gaussian model error  $\mathbf{w}_i$  with an error covariance matrix of  $\mathbf{Q}_i$  (Eq. 2), the forecast error covariance  
 10  $\mathbf{P}_i^-$  can be approximated by:

$$11 \quad \mathbf{P}_i^- = \mathbf{F}_{i,i-1} \mathbf{P}_{i-1}^+ \mathbf{F}_{i,i-1}^T + \mathbf{Q}_i \quad (16)$$

12 where  $\mathbf{F}_{i,i-1}$  (2x2) is a linearized version of  $\mathbf{f}_{i,i-1}(\cdot)$  and  $\mathbf{F}_{i,i-1} \mathbf{P}_{i-1}^+ \mathbf{F}_{i,i-1}^T$  is the propagated analysis error  
 13 covariance. In using a tangent linear  $\mathbf{F}_{i,i-1}$  operator, the method is referred to as ‘Extended’ Kalman  
 14 filter. If  $\mathbf{F}_{i,i-1}$  is a linearized model version, then Eq. (16) is known to suffer from unlimited error  
 15 variance growth, because the third and higher order moments of the Taylor expansion are discarded  
 16 in Eq. (16) (closure problem). It is possible to avoid these problems with other Kalman filter  
 17 variants, as discussed in the next sections.

18

19



### 6.1.3 Soil Moisture (Retrieval) Data Assimilation Illustrated with 1D Ensemble Kalman Filtering

The ensemble Kalman filter (EnKF, *Reichle et al. 2002*) circumvents the need for a linear(-ized) state propagation model and observation operator by diagnosing error covariance matrices from ensemble information. Examples of one-dimensional (“1D”) EnKF studies using soil moisture retrievals from various microwave sensors include *Liu et al (2011)* and *Draper et al (2012)*. A “1D” EnKF updates the state at the locations that coincide with the assimilated observations and it is assumed that the observations and the model have the same spatial resolution. In the next section (6.1.4) a spatially distributed or three-dimensional (“3D”) expansion of the EnKF will be presented, with inclusion of horizontal information propagation and with the ability to possibly deal with multiple scales.

Assume again that satellite-based surface soil moisture retrievals  $\text{sfmc}_{\text{obs}}$  are assimilated and that the model operates at the same spatial resolution as the observations. An ensemble of states  $\hat{\mathbf{x}}_{i,j}^-$  ( $j=1,\dots,N$ ) is generated by perturbing the model simulations (discussed in section 7.2.1). The observations are also perturbed to ensure consistency in the EnKF formulation used here. Note though that some variants of the EnKF exist that avoid such perturbations. The observation predictions are given by  $\hat{\mathbf{y}}_{i,j}^- = \widehat{\text{sfmc}}_{i,j}^- = h(\hat{\mathbf{x}}_{i,j}^-)$ , i.e. accounting for a possibly non-linear mapping between the observed  $\text{sfmc}_{\text{obs},i,j}$  and the state variables, even though in this example the observation operator is linear  $\mathbf{H} = [1 \ 0]$ . The update equation for each state member can be written as:

$$\left[ \widehat{\text{sfmc}} \right]_{i,j}^+ = \left[ \widehat{\text{sfmc}} \right]_{i,j}^- + \mathbf{K}_i [\text{sfmc}_{\text{obs}} - \widehat{\text{sfmc}}^-]_{i,j}, \text{ with} \quad (17)$$

$$\mathbf{K}_i = \text{Cov}(\hat{\mathbf{x}}_i^-, \hat{\mathbf{y}}_i^-) [\text{Cov}(\hat{\mathbf{y}}_i^-, \hat{\mathbf{y}}_i^-) + \mathbf{R}_i]^{-1} = \text{Cov}(\hat{\mathbf{x}}_i^-, \hat{\mathbf{y}}_i^-) [\sigma_{\text{sfmc}}^2 + \sigma_{\text{sfmc,obs}}^2]_i^{-1} \quad (18)$$

Unlike Eq. (16), the error covariances used in the Kalman gain are now dynamically diagnosed from the ensemble dispersion in the forecasts and observation predictions. Specifically,  $\text{Cov}(\hat{\mathbf{x}}_i^-, \hat{\mathbf{y}}_i^-)$  is found by correlating the ensemble departures in the state variables with those in the observation predictions and  $\text{Cov}(\hat{\mathbf{y}}_i^-, \hat{\mathbf{y}}_i^-)$  is the error covariance of the observation predictions. Note that  $\mathbf{P}_i^- = \text{Cov}(\hat{\mathbf{x}}_i^-, \hat{\mathbf{x}}_i^-)$ , but the computation of this matrix is not required for the Kalman gain (Eq. 18). The gain factor  $\mathbf{K}_i$  maps the surface soil moisture *innovation*  $[\text{sfmc}_{\text{obs}} - \widehat{\text{sfmc}}^-]_i$  to *increments*  $\mathbf{K}_i[\text{sfmc}_{\text{obs}} - \widehat{\text{sfmc}}^-]_i$  in all prognostic state variables, using the diagnosed error covariances between these variables.

The final a posteriori state estimate  $\hat{\mathbf{x}}_i^+$  and its uncertainty are given by:

$$[\widehat{\text{sfmc}}_{\text{rzmc}}^+]_i = \frac{1}{N} \sum_{j=1}^N [\widehat{\text{sfmc}}_{\text{rzmc}}^+]_{i,j} \quad \text{with } \mathbf{P}_i^+ = \text{Cov}(\hat{\mathbf{x}}_i^+, \hat{\mathbf{x}}_i^+) \quad (19)$$

The a posteriori uncertainty in the state estimate  $\mathbf{P}_i^+$  is diagnosed from the analysis ensemble, which typically contracts during the assimilation.

#### 6.1.4 Brightness Temperature Assimilation Illustrated with 3D Ensemble Kalman Filtering

Classical retrieval assimilation is appealing because of its relatively straightforward implementation, but there is a serious concern about observation biases. The inversion process from brightness temperatures to soil moisture retrievals relies on parameters and ancillary

information that may be inconsistent with that used in the land surface model within in the assimilation system. It is thus more natural to couple a radiative transfer or backscatter model to a land surface model, forecast  $\widehat{Tb}_c^-$  or  $\widehat{\sigma}_c^{0-}$  along with soil moisture, and then assimilate  $Tb_{c,obs}$  or  $\sigma_{c,obs}^0$  (rather than the soil moisture retrievals) as in *Entekhabi et al. (1994)*, *Reichle et al. (2001)* and *Balsamo et al. (2006)*, amongst others.

In the following example, the above EnKF equations are further illustrated for spatial (or “3D”) filtering (*Reichle and Koster, 2003*) and using brightness temperature observations  $Tb_{obs}$  at a coarser resolution than the fine-scale model simulations. This will highlight that (i) brightness temperature information can be translated into soil moisture updates, (ii) soil moisture can be updated in unobserved areas, and (iii) fine-scale soil moisture estimates can be obtained, through dynamic disaggregation of coarse-scale observations. The observation predictions  $\widehat{Tb}_i^-$  require model information about soil moisture, temperature and vegetation. The state vector therefore contains surface and soil temperature and possibly vegetation, especially if the latter is dynamically evolving in the model. Yet, here it is excluded for simplicity.

The state update is presented at a single fine-scale location  $k$ , and a single ensemble member  $j$ , using (possibly multiple) coarse-scale observations  $Tb_{obs,\kappa}$  ( $\kappa = 1, \dots, m$ ) that are within a chosen influence area around the fine-scale location, as illustrated in Figure 2:

$$1 \quad \begin{bmatrix} \widehat{\text{sfmt}}_{i,j} \\ \widehat{\text{rzmc}}_{i,j} \\ \widehat{\text{tsurf}}_{i,j} \\ \widehat{\text{tsoil}}_{i,j} \end{bmatrix}_k^+ = \begin{bmatrix} \widehat{\text{sfmt}}_{i,j} \\ \widehat{\text{rzmc}}_{i,j} \\ \widehat{\text{tsurf}}_{i,j} \\ \widehat{\text{tsoil}}_{i,j} \end{bmatrix}_k^- + [\mathbf{K}_i]_k \left( \begin{bmatrix} \text{Tb}_1 \\ \dots \\ \text{Tb}_k \\ \dots \\ \text{Tb}_m \end{bmatrix}_{\text{obs}} - \begin{bmatrix} \widehat{\text{Tb}}_1 \\ \dots \\ \widehat{\text{Tb}}_k \\ \dots \\ \widehat{\text{Tb}}_m \end{bmatrix}_{i,j}^- \right) \quad (20)$$

2 The coarse-scale observation predictions are calculated by (i) transforming the fine-scale model  
3 state variables into fine-scale  $\widehat{\text{Tb}}_{i,j,k}^- = \mathbf{h}_p([\hat{\mathbf{x}}_{i,j}^-]_k)$  using a radiative transfer model  $\mathbf{h}_p(\cdot)$  and (ii)  
4 aggregating the fine-scale  $\widehat{\text{Tb}}_{i,j,k}^-$  ( $k=1, \dots, N_k$ ) to a coarse-scale  $\widehat{\text{Tb}}_{i,j,k}^-$  (Figure 2a). The observation  
5 operator  $\mathbf{h}(\cdot)$  combines these two operations, so that:

$$6 \quad \hat{\mathbf{y}}_{i,j}^- = \mathbf{h}(\hat{\mathbf{x}}_{i,j}^-) = \begin{bmatrix} \widehat{\text{Tb}}_1 \\ \dots \\ \text{Tb}_k \\ \dots \\ \text{Tb}_m \end{bmatrix}_{i,j}^- = \begin{bmatrix} \frac{1}{N_1} \sum_{k=1}^{N_1} \mathbf{h}_p([\hat{\mathbf{x}}_{i,j}^-]_k) \\ \dots \\ \frac{1}{N_k} \sum_{k=1}^{N_k} \mathbf{h}_p([\hat{\mathbf{x}}_{i,j}^-]_k) \\ \dots \\ \frac{1}{N_m} \sum_{k=1}^{N_m} \mathbf{h}_p([\hat{\mathbf{x}}_{i,j}^-]_k) \end{bmatrix} \quad \text{with } [\hat{\mathbf{x}}_{i,j}^-]_k = \begin{bmatrix} \widehat{\text{sfmt}}_{i,j} \\ \widehat{\text{rzmc}}_{i,j} \\ \widehat{\text{tsurf}}_{i,j} \\ \widehat{\text{tsoil}}_{i,j} \end{bmatrix}_k^- \in \hat{\mathbf{x}}_{i,j}^- . \quad (21)$$

7 The Kalman gain to update each fine-scale  $[\hat{\mathbf{x}}_{i,j}^-]_k$  is found as:

$$8 \quad [\mathbf{K}_i]_k = \text{Cov}([\hat{\mathbf{x}}_i^-]_k, \hat{\mathbf{y}}_i^-) [\text{Cov}(\hat{\mathbf{y}}_i^-, \hat{\mathbf{y}}_i^-) + \mathbf{R}_i]^{-1} \quad (22)$$

9 where  $\text{Cov}([\hat{\mathbf{x}}_i^-]_k, \hat{\mathbf{y}}_i^-)$  is the error covariance between the fine-scale state variables and the coarse-  
10 scale observation predictions. The Kalman gain thus effectively partitions (Figure 2b) the  
11 information in the coarse-scale  $\text{Tb}_{\text{obs}}$  observations to fine-scale increments in soil moisture and  
12 temperature, using the error cross-correlations between fine-scale state variables, such as soil  
13 moisture, and coarse-scale  $\widehat{\text{Tb}}_k^-$  observation predictions. The satellite-observed  $\text{Tb}_{\text{obs}}$  only provides  
14 information about the top ( $\sim 5$  cm) layer soil moisture, but data assimilation propagates this surface

information to deeper soil moisture layers through the model soil profile dynamics and the vertical error correlations between state variables.

The added advantage of 3D filtering is primarily in data-sparse regions, because information is horizontally propagated through the spatial forecast error structure. The spatial error correlations that are expressed in the off-diagonal elements of the cross-covariance matrix  $\text{Cov}([\hat{\mathbf{x}}_i^-], \hat{\mathbf{y}}_i^-)$  allow updating the state  $[\hat{\mathbf{x}}_{i,j}^-]_k$  at the fine-scale location  $k$  with surrounding multiple coarse-scale innovations, as long as the latter are within the influence area around the fine-scale location (even if the state variable  $[\hat{\mathbf{x}}_{i,j}^-]_k$  is ‘unobserved’ and not part of any coarse-scale observation prediction). The influence area is typically obtained by localizing the spatial error correlations (discussed in section 7.2.1) to limit the impact of distant observations.

Finally, it should be noted that the (spatial) observation vector can be further expanded by assimilating multiple types of observations simultaneously. For example, brightness temperatures are typically observed at two polarizations (H and V), and possibly at multiple incidence angles (e.g. SMOS). A 3D EnKF using both H- and V-polarized brightness temperatures is used for an operational SMAP data assimilation product as discussed in section 9.2.

## 6.2 Smoothing

Smoothers update state vectors that are distributed in time. Smoothers have the potential to improve soil moisture re-analyses by assimilating multiple observations in time or time-integrated observations, such as, for example, TWS or river discharge. Here, a smoother is illustrated for the assimilation of monthly coarse-scale TWS as an extension of a spatially distributed (“3D”) ensemble Kalman filter in which the fine-scale state is distributed in time. The relevant model prognostic variables included in the state vector are the depth to the ground water table (gwt) and root-zone soil moisture (rzmc). The concept is first introduced by updating each member  $j$  of the time-augmented ( $i=1,\dots,T$ ) state vector at a fine-scale location  $k$  using the traditional ensemble Kalman filter equations:

$$\begin{bmatrix} \widehat{\text{gwt}}_{1,j} \\ \text{rzmc}_{1,j} \\ \dots \\ \text{gwt}_{i,j} \\ \text{rzmc}_{i,j} \\ \dots \\ \text{gwt}_{T,j} \\ \text{rzmc}_{T,j} \end{bmatrix}_k^+ = \begin{bmatrix} \widehat{\text{gwt}}_{1,j} \\ \text{rzmc}_{1,j} \\ \dots \\ \text{gwt}_{i,j} \\ \text{rzmc}_{i,j} \\ \dots \\ \text{gwt}_{T,j} \\ \text{rzmc}_{T,j} \end{bmatrix}_k^- + [\mathbf{K}]_k \left( \begin{bmatrix} \text{TWS}_1 \\ \dots \\ \text{TWS}_\kappa \\ \dots \\ \text{TWS}_m \end{bmatrix}_{\text{obs}} - \begin{bmatrix} \widehat{\text{TWS}}_1 \\ \dots \\ \text{TWS}_\kappa \\ \dots \\ \text{TWS}_m \end{bmatrix}_j^- \right) \quad (23)$$

The coarse-scale monthly (time index omitted) observation predictions ( $\kappa = 1,\dots,m$ ) are obtained by first calculating fine-scale vertically integrated TWS using  $\mathbf{h}_{\text{TWS}}(\cdot)$  and then aggregating the fine-scale state variables in space ( $k=1,\dots, N_\kappa$ ) and time ( $i=1,\dots,T$ ):

$$\hat{\mathbf{y}}_j^- = \mathbf{h}(\hat{\mathbf{x}}_j^-) = \begin{bmatrix} \widehat{\text{TWS}}_1 \\ \dots \\ \text{TWS}_\kappa \\ \dots \\ \text{TWS}_m \end{bmatrix}_j^- = \begin{bmatrix} \frac{1}{T} \frac{1}{N_1} \sum_{k=1}^{N_1} \sum_{i=1}^T \mathbf{h}_{\text{TWS}} \left( [\hat{\mathbf{x}}_{i,j}^-]_k \right) \\ \dots \\ \frac{1}{T} \frac{1}{N_\kappa} \sum_{k=1}^{N_\kappa} \sum_{i=1}^T \mathbf{h}_{\text{TWS}} \left( [\hat{\mathbf{x}}_{i,j}^-]_k \right) \\ \dots \\ \frac{1}{T} \frac{1}{N_m} \sum_{k=1}^{N_m} \sum_{i=1}^T \mathbf{h}_{\text{TWS}} \left( [\hat{\mathbf{x}}_{i,j}^-]_k \right) \end{bmatrix} \quad \text{with } [\hat{\mathbf{x}}_{i,j}^-]_k = \begin{bmatrix} \widehat{\text{gwt}}_{i,j} \\ \text{rzmc}_{i,j} \\ \dots \end{bmatrix}_k^- \quad (24)$$

The above update Eq. (23) could potentially involve a large-dimensional Kalman gain for which the error covariances are only valid if the number of included time steps (T) is small relative to the ensemble size, as in *Dunne and Entekhabi (2006)* who assimilated a batch of temporally distributed soil moisture observations and in *Pauwels and De Lannoy (2006)* who assimilated time-integrated discharge observations. Alternatively, and in analogy with strong constraint variational assimilation ([Chapter X632X](#)), one can limit the update to the initial conditions at the beginning (timestep i0) of the assimilation window ( $\hat{\mathbf{x}}_{i0,j,k}^-$ ) so that the model trajectory over the entire smoothing window best fits the observations. The  $[\mathbf{K}_1]_k$  matrix then becomes:

$$[\mathbf{K}_{i0}]_k = \text{Cov}([\hat{\mathbf{x}}_{i0}]_k, \hat{\mathbf{y}}^-) [\text{Cov}(\hat{\mathbf{y}}^-, \hat{\mathbf{y}}^-) + \mathbf{R}]^{-1} \quad (25)$$

Yet, adding a full increment to the initial soil moisture state  $\hat{\mathbf{x}}_{i0,k,j}^-$  alone will not cause the desired persistent trajectory shift in hydrologic models. Instead, *Zaitchik et al., 2008* computed an effective increment at each timestep i by equally distributing the increment over the T time steps in the smoothing window, so that:

$$[\hat{\mathbf{x}}_{i,j}^+]_k = [\hat{\mathbf{x}}_{i,j}^-]_k + \frac{1}{T} [\mathbf{K}_{i0}]_k \left( \begin{bmatrix} \text{TWS}_1 \\ \dots \\ \text{TWS}_k \\ \dots \\ \text{TWS}_m \end{bmatrix}_{\text{obs}} - \begin{bmatrix} \widehat{\text{TWS}}_1 \\ \dots \\ \widehat{\text{TWS}}_k \\ \dots \\ \widehat{\text{TWS}}_m \end{bmatrix}^- \right)_j, \text{ for each } i = 1, \dots, T \quad (26)$$

The TWS innovations are thus partitioned in time and space and into different water storage components. The methodological development for smoothing GRACE observations in the context of soil moisture assimilation is still in its infancy. Alternative formulations are under investigation.

### 6.3 Joint State and Parameter Updating

The above examples update the land surface state in response to observations related to soil moisture. The term ‘data assimilation’ can also be used to estimate model parameters using observations related to soil moisture. Such parameter estimates could be static, as typically obtained after optimization of long-term statistics that involve differences between long time series of simulations and observations. Slowly varying parameters could be updated dynamically through recursive filtering, using similar techniques as described above, but after replacing (i) the state variables with parameters and (ii) the prognostic state propagation model with a persistent model. A combined state and parameter estimation has also been explored (e.g. *Montzka et al., 2013*), but not for large-scale soil moisture modeling systems: the realism and observability of evolving parameters in interaction with dynamic state updates may pose difficulties.

## 7. Random Errors and Biases

The key to successful data assimilation is to qualify and quantify the errors in the model forecasts and observations. The errors include both random and systematic error, or bias. In the absence of knowledge about the true ensemble error at each time instant or location, land surface modelers often turn to the ergodicity principle and analyze errors in time series or spatial patterns. In that sense, bias can be defined as autocorrelated error, and the correlation length determines the temporal or spatial scale of bias. For large-scale (continental, global) hydro-meteorological modeling, random errors have autocorrelation lengths of less than a few days in time (microscale, mesoscale), whereas bias or systematic error has time scales of several weeks or more. The



following sections discuss the treatment of random errors and biases specifically for soil moisture data assimilation.

### *7.1 Bias, Autocorrelated Error*

Statistically ‘optimal’ data assimilation techniques, such as Kalman filtering, rely on observations and forecasts with zero-mean errors (first moment). A typical problem with assimilating satellite observations of soil moisture, however, is that their climatology differs from that of the land model integrations. If biases cannot be addressed through model calibration, then one can either treat the bias a priori and perform anomaly assimilation (i.e. after mapping the observations to the model climatology) or estimate the bias dynamically inside the assimilation scheme. Either approach to dealing with bias reduces the average magnitude of the innovations and avoids that the model is pushed away from its own climatology through data filtering. The climatological rescaling techniques are based on a priori knowledge and thus require historical data, whereas on-line bias estimation methods update the bias estimates dynamically at each assimilation event. Another difference is that rescaling techniques could address discrepancies between datasets in higher order moments under the assumption of stationary differences in the first moment, whereas the on-line bias estimation methods are focused on resolving non-stationary differences in the first moments.

#### 7.1.1. A Priori Static Bias Treatment

A commonly used approach in soil moisture assimilation systems is to remove long-term differences between observations and forecasts by rescaling the observations to the model

climatology. Rescaling does not per se assign the systematic errors to either the model or the observations, but rather removes the total bias from the innovations.

A first approach to rescaling is to match the cumulative distribution function (CDF) of observed soil moisture values to the CDF of the soil moisture simulations (*Reichle and Koster, 2004; Drusch et al., 2005*), thereby matching the long-term first, second and higher order moments of the observations to the model. Figure 3a illustrates the CDF-matching approach. CDFs are calculated using a multi-year historical data set of observations and land surface simulations for each location in space. This is illustrated by sampling SMOS retrievals and GEOS-5 simulations for ascending orbits (6:00 am local time) at a 36 km grid cell inside the Walnut Gulch watershed in Arizona (US). To complement the temporal sampling, additional sampling is performed in a spatial window, which effectively smoothes the statistics. Here, all 36 km grid cells within a  $0.5^\circ$  radius around the central Walnut Gulch pixel are sampled. In this example, the SMOS retrievals are systematically drier than the simulations. To rescale an individual soil moisture retrieval (e.g. at  $0.075 \text{ m}^3/\text{m}^3$ ), the cumulative probability density for this value is found (e.g. 0.62 [-]). Then, this probability is transferred to the model CDF and the corresponding modeled soil moisture (e.g.  $0.12 \text{ m}^3/\text{m}^3$ ) is found. In practice, this mapping happens by fitting a relationship between the observed and simulated soil moisture at identical cumulative probability densities. The observation rescaling possibly involves a change in the dynamical range of the observations and therefore it is important to also rescale the original observation errors ( $\mathbf{R}$ ). The error standard deviation  $\sigma_{\text{sfmc,obs}}$  is rescaled to  $\sigma'_{\text{sfmc,obs}}$ , using the long-term (climatological) standard deviation of the observations  $S[\text{sfmc}_{\text{obs}}]$  and simulations  $S[\widehat{\text{sfmc}}^-]$ , i.e.

$$\sigma'_{\text{sfmc,obs}} = \sigma_{\text{sfmc,obs}} \cdot S[\widehat{\text{sfmc}}^-] / S[\text{sfmc}_{\text{obs}}] \quad (27)$$

The static nature of the CDF-matching approach is not always ideal, because it discards seasonal cycles in biases and may therefore even introduce biases into the system. In some applications, the CDF-matching approach has therefore been applied by season (*de Rosnay et al., 2014*).

The seasonality in biases is of particular concern when assimilating brightness temperatures, which are strongly impacted by seasonally varying surface temperature (section 9.2). When it is important to resolve the seasonal and diurnal cycles of the climatology, rescaling is usually limited to the first moment and possibly the second moment, rather than the complete CDF, due to the limited availability of historical data. Figure 3b illustrates temporally variable biases between multi-year averaged brightness temperatures from SMOS at 40° incidence angle and simulations with the GEOS-5 land system, both at 6:00 am local time (ascending overpass). The temporally variable climatology of the mean brightness temperature is calculated by temporally smoothing the datasets (with the model crossmasked for the availability of observations), and calculating a mean brightness temperature for each pentad (5-day period) averaged across 3 years. The climatological mean values of observed and modeled brightness temperature for each pentad  $p$  are given by  $\langle \text{Tb}_{\text{obs},p} \rangle$  and  $\langle \widehat{\text{Tb}}_p^- \rangle$ . Each individual  $\text{Tb}_{\text{obs},i}$  observation is then rescaled to  $\text{Tb}'_{\text{obs},i}$  using climatological information from the closest pentad  $p$ :

$$\text{Tb}'_{\text{obs},i} = \text{Tb}_{\text{obs},i} - \langle \text{Tb}_{\text{obs},p} \rangle + \langle \widehat{\text{Tb}}_p^- \rangle = \text{Tb}_{\text{obs\_anom},i} + \langle \widehat{\text{Tb}}_p^- \rangle \quad (28)$$

where  $Tb_{obs\_anom,i}$  is the anomaly of the assimilated observations. The observation predictions can be similarly written as  $\widehat{Tb}_i^- = \widehat{Tb}_{anom,i}^- + \langle \widehat{Tb}_p^- \rangle$ , with  $\widehat{Tb}_{anom,i}^-$  denoting the anomaly in the simulations. Consequently, the innovations can be written as:

$$Tb'_{obs,i} - \widehat{Tb}_i^- = Tb_{obs\_anom,i} - \widehat{Tb}_{anom,i}^- \quad (29)$$

This effectively means that anomaly information is assimilated when a rescaling approach is implemented.

#### 7.1.2. On-Line Dynamic Bias Estimation

Bias can be estimated dynamically inside the data assimilation system, using information in the innovations. Without knowledge of the origin of persistent errors in the innovations, it is impossible to assign the bias to state forecast errors or observation errors.

Observation bias estimation removes bias from the innovations, and leaves the model and assimilation output in its own climatology. Similarly to observation rescaling techniques, dynamic observation bias estimation effectively aims at anomaly assimilation. The difference is that the climatological differences between the observation predictions and observations (e.g.  $\langle \widehat{Tb}_p^- \rangle - \langle Tb_{obs,p} \rangle$  in Eq. 28) are replaced by temporally variable bias estimates  $\widehat{b}_i^{obs}$  at each assimilation time step  $i$ . As an example, the state update equation (Eq. 5) would become:

$$\hat{\mathbf{x}}_i^+ = \hat{\mathbf{x}}_i^- + \mathbf{K}_i [\mathbf{y}_{obs,i} - \mathbf{h}_i(\hat{\mathbf{x}}_i^-) - \widehat{\mathbf{b}}_i^{obs}] \quad (30)$$

Forecast bias estimation techniques, on the other hand, remove state bias from the innovations (similar to rescaling techniques) and correct the model simulations for bias (i.e. they assign bias to the model, unlike rescaling techniques), either only in post-processing or with feedback into the model. Given a dynamic estimate of the forecast bias  $\widehat{\mathbf{b}}_i^f$ , the state update equation will be:

$$\hat{\mathbf{x}}_i^+ = (\hat{\mathbf{x}}_i^- - \widehat{\mathbf{b}}_i^f) + \mathbf{K}_i [\mathbf{y}_{\text{obs},i} - \mathbf{h}_i(\hat{\mathbf{x}}_i^- - \widehat{\mathbf{b}}_i^f)] \quad (31)$$

For soil moisture data assimilation, the on-line forecast bias estimation technique has only been used in small-scale research studies (*De Lannoy et al, 2007*), but not yet in large-scale or operational applications. Forecast bias estimation and a correction of soil moisture simulations is particularly useful if knowledge of absolute levels of soil moisture is important in addition to knowledge of the temporal evolution of soil moisture. However, the main problem is that simple forecast bias models do not allow to propagate information from observed (e.g. surface soil moisture) to unobserved (e.g. root-zone soil moisture) variables.

## 7.2 Random Error

The observation and forecast error covariances (second moments) determine the relative weight of the observations in the assimilation scheme as well as the spatial (horizontal and vertical) distribution of the analysis increments. The optimality of data assimilation system depends on how these uncertainties are defined upon input.

### 7.2.1. Forecast Error Covariance

The various data assimilation techniques described above differ in how they handle the forecast error covariance matrix  $\mathbf{P}_i^-$ . For soil moisture assimilation, ensemble simulations have arguably become the most popular method to dynamically estimate the forecast error variance and the inter-variable error correlations (*Reichle et al., 2002*). This approach is also most directly relevant for ensemble hydro-meteorological forecasting ([Chapter X650,649X](#)). In ensemble soil moisture assimilation, the ensemble is usually generated by perturbing the forcings, model prognostic variables and possibly land model parameters. In practice, the data assimilation system is calibrated by tuning magnitude of the perturbations to ensure that the innovations and increments show the expected behavior (section 7.2.3) and the assimilation results perform well (section 8). Some a priori ensemble verification (*De Lannoy et al., 2006*, [Chapter X484X](#)) could also be performed before activating the data assimilation. Good ensembles should envelop the observations with an ensemble standard deviation that is comparable to the root-mean-square-error between the ensemble mean predictions and the observations.

Perturbations to model forcing and prognostic variables are usually applied at regular time intervals during the model integration, because the dispersion in soil moisture simulations is bounded and would collapse unless model forcing or prognostic variables are applied. Alternatively, perturbing land model parameters ensures a persistent ensemble spread, but this approach creates temporal error autocorrelation and may not reflect random errors properly.

As an example, Table 2 shows preliminary perturbations that are currently used for brightness temperature assimilation in the GEOS-5 land data assimilation system (section 9.2). Select model

1 prognostic variables and forcings are perturbed at each model time step, and land model parameters  
2 are not perturbed. Perturbations to radiation, temperature and humidity are normally distributed  
3 and additive, whereas precipitation perturbations are lognormally distributed and multiplicative,  
4 because of the skewed nature of precipitation distributions. The forcing perturbations are applied  
5 with a temporal autocorrelation of 1 day and a spatial correlation scale of 50 km. Perturbations to  
6 the soil moisture (catdef, rzexc, srfexc) model prognostic variables (section 4) are additive and  
7 applied with shorter correlation scales in space and time. Soil temperature is not explicitly  
8 perturbed to avoid excessive ensemble spreads in areas without vegetation, but it is indirectly  
9 perturbed through the perturbation of the radiation. Cross-correlations are also imposed to ensure  
10 some physical realism between the perturbed fields. The ensemble mean for all perturbations is  
11 constrained to zero for additive perturbations and to one for multiplicative perturbations.

12  
13 When spatial filtering is applied, spatial error correlations are critical to ensure meaningful updates  
14 to the fine-scale state variables. The coarse-scale observation prediction error variance obtained  
15 by spatially aggregating  $N$  independent fine-scale state variables equals the fine-scale error  
16 variance divided by  $N$ , i.e. aggregation causes a reduction in uncertainty. With inclusion of  
17 appropriate spatial correlations the spatially aggregated uncertainty of the observation predictions  
18 is effectively increased. The same holds for temporal smoother applications, where temporal  
19 autocorrelation is important to ensure sufficient uncertainty in the observation predictions (relative  
20 to the observations).

21  
22 As opposed to the useful spatial autocorrelations, the spurious long-range correlations are  
23 detrimental statistical artifacts in diagnosed ensemble  $\mathbf{P}_i^-$  matrices. To limit these spurious

correlations and to reduce the undesirable impact of distant observations, ensemble filter techniques mostly include some covariance localization (*Reichle and Koster 2003*). Correlations beyond a certain separation distance are suppressed by using a Hadamard product with a local compactly supported correlation function that reaches zero beyond a given distance. This product is applied to the sample covariance terms  $\text{Cov}(\hat{\mathbf{x}}_i^-, \hat{\mathbf{y}}_i^-)$  and  $\text{Cov}(\hat{\mathbf{y}}_i^-, \hat{\mathbf{y}}_i^-)$  in the expression for the Kalman gain.

Finally, the number of ensemble members needs to allow a statistically valid diagnosis of the forecast error covariance matrix and should thus increase with the number of variables in the state. Most soil moisture assimilation applications use 10-100 ensemble members.

#### 7.2.2. Observation Error Covariance

Observation uncertainty refers to all errors present in observation space, i.e. uncertainty due to sensor error, retrieval error, and representativeness error. Sensor error is given by instrument design specifications. For example, the Microwave Imaging Radiometer with Aperture Synthesis instrument onboard SMOS measures multi-angular brightness temperatures with a radiometric error of 4 K (*Kerr et al., 2010*), and the radiometer onboard SMAP is designed to measure brightness temperatures at a single 40° incidence angle with an error of 1.3 K (*Entekhabi et al., 2014*). Retrieval error depends on the radiative transfer or backscattering model, dynamic auxiliary information and parameters. Representativeness error is often due to a horizontal or vertical mismatch between the observation and the observation predictions. For example, a collection of model grid cells may not accurately capture the actual sensor field of view area. Moreover, the penetration depth of microwaves decreases with increasing soil moisture content,



whereas the simulated soil moisture is valid for a surface layer with a fixed thickness. Observation error also includes representativeness errors in the observation operator  $\mathbf{h}_i(\cdot)$ . This error specifically refers to uncertainty in the observation operator (e.g. due to erroneous parameters) and does not include errors in the state forecast  $\hat{\mathbf{x}}_i^-$ . One promising method to obtain an estimate of soil moisture observation errors is the triple collocation procedure (*Scipal et al. 2008*). This method uses three independent estimates of soil moisture in order to estimate the uncertainty in one of them. However, the success of this method relies on conditions that are often difficult to meet in practice.

### 7.2.3. Error Optimization and Adaptive Filtering

The specification of error parameters as input to the data assimilation system is often user-defined and not necessarily optimal. The innovations provide a means to assess the filter behavior: for a linear system, the innovations should have a Gaussian distribution with zero mean and a covariance of  $[\mathbf{H}\mathbf{P}^-\mathbf{H}^T + \mathbf{R}]_i$ . In practice, land surface models are non-linear and the Gaussian assumption is difficult to meet. However, the consistency of the innovations with the imposed a priori error covariances and observation error covariances (*Reichle et al., 2002*) can be (approximately) verified by normalizing the (ensemble mean) innovation  $\langle \mathbf{y}_{\text{obs},i} - \mathbf{H}_i \hat{\mathbf{x}}_i^- \rangle$  for each point in space and at each assimilation time step by the imposed  $[\mathbf{H}\mathbf{P}^-\mathbf{H}^T + \mathbf{R}]_i$ . The distribution of these normalized innovations (in time and/or space, ergodic sampling) should follow a normal distribution. If the standard deviation is less (larger) than one, then the values for  $\mathbf{R}_i$  and/or  $\mathbf{P}_i^-$  are too large (small). This can be used to manually optimize the filter. The alternative is to automatically tune the forecast error covariance  $\mathbf{P}_i^-$ , or more specifically the model error

component  $Q_i$ , during the on-line cycling of the data assimilation system through adaptive filtering (Crow and Yilmaz, 2014). However, the adaptive methods have not yet been thoroughly tested for large-scale data assimilation systems.

#### 7.2.4. Analysis Error Covariance

A typical feature of data assimilation is that it reduces the analysis errors, both in terms of ensemble errors and in time series errors (see section 8). Figure 4 illustrates how the ensemble analysis uncertainty in GEOS-5 simulated soil moisture is reduced compared to the forecast uncertainty, with a globally averaged fraction of 0.8, when assimilating SMOS retrievals during the period July 2010 – July 2013.

## **8. Evaluation of Soil Moisture Estimates from Data Assimilation**

### *8.1 In Situ Soil Moisture*

Large-scale soil moisture data assimilation results are typically validated with in situ soil moisture observations, or some other measurements that depend on soil moisture, such as turbulent fluxes or river discharge. This section specifically focuses on validation against independent in situ soil moisture measurements, i.e. observations that were not used in the data assimilation.

The most accurate measurements of soil moisture involve collecting soil samples that are weighed before and after drying to determine the amount of water present in the soil matrix. Yet, such destructive gravimetric measurements cannot be frequent in time or space and therefore, they

1 mainly serve to calibrate automated in situ soil moisture measuring devices, such as capacitance  
2 probes, time domain reflectometry probes and neutron probes. Across the world, thousands of  
3 measurement stations are equipped with soil probes that record time series of soil moisture at  
4 various depths in the ground. Select examples of networks with more than 50 soil moisture  
5 measuring sites are the US Natural Resources Conservation Service Soil Climate Analysis  
6 Network (SCAN), the SNOwpack TELemetry network (SNOTEL) and the US Climate Reference  
7 Network (USCRN). Other in situ soil moisture networks include the cosmic-ray soil moisture  
8 observing system (COSMOS) and global positioning system receivers (GPS), both of which use  
9 relationships between signals collected above the ground and vertically and horizontally integrated  
10 soil moisture, rather than using probes inserted in the ground. The limited spatial support of the  
11 point measurements complicates the comparison of spatial patterns or absolute values against  
12 gridded regional or global LSM simulations. However, the temporal variability in soil moisture at  
13 point locations provides useful information to validate the dynamics of model and assimilation  
14 results.

15  
16 In addition, some watershed-averaged in situ measurements of surface soil moisture are available  
17 from core validation sites (*Entekhabi et al., 2014, Chapter 7, p.119-150*) listed in Table 3. These  
18 USDA watersheds are equipped with locally dense sensor networks covering the area of a satellite  
19 footprint, which makes them directly relevant for the validation of remote sensing retrievals, but  
20 are also very attractive to validate coarse-scale model or assimilation results. Table 3 provides  
21 details about the 36 km reference grid cells that are identified within each watershed for the

evaluation of SMOS data assimilation in the example of section 8.3 below. The soil moisture in each reference grid cell is computed as the average soil moisture across at least 5 profile sensors.

## 8.2 Validation Metrics

A number of metrics exist to validate simulation and assimilation results with in situ observations. It is often advised to focus on the temporal variability and use bias-free metrics for two reasons: (i) a comparison of gridded coarse-scale model output against point-scale in situ observations will suffer from representativeness biases and (ii) data assimilation for state updating alone is meant to correct for random errors and is not designed to fix any long-term biases between the model and observations. Examples of suitable metrics include the unbiased root-mean-square-error (ubRMSE) (*Entekhabi et al., 2010, Albergel et al., 2013*) and the anomaly correlation coefficient.

The RMSE between time series ( $i=1, \dots, T$ ) of simulated soil moisture content ( $mc_{est}$ , either forecasts or analyses) and in situ soil moisture measurements ( $mc_{insitu}$ ) can be expanded as

$$RMSE = \sqrt{\frac{1}{T} \sum_{i=1}^T (mc_{est,i} - mc_{insitu,i})^2} \quad (32)$$

$$= \sqrt{S^2[mc_{est}] + S^2[mc_{insitu}] - 2 \cdot R \cdot S[mc_{est}] \cdot S[mc_{insitu}] + bias^2} \quad (33)$$

where  $S[.]$  is the temporal standard deviation,  $R$  is the time series correlation coefficient and ‘bias’ is the difference between the long-term mean simulations and observations. This metric thus

focuses on both similarities in temporal variability and on bias. The ubRMSE removes the bias term, or

$$\text{ubRMSE}^2 = \text{RMSE}^2 - \text{bias}^2 \quad (34)$$

and measures only the random error component of the RMSE. The anomaly time series correlation coefficient measures the linear correlation between simulations and observations after subtracting their respective seasonal climatologies, i.e. seasonally varying climatological mean values are subtracted from each data point. The temporal mean of the anomalies is zero by definition. The climatologies are obtained by smoothing the datasets (for a particular time of day, in case subdiurnal output is validated), and then calculating a multi-year average ( $\overline{(\cdot)}_{(i)}$ ) for each day, week, or month, depending on the temporal resolution. Note that the calculation of a climatology requires at least a few years of data. The anomaly correlation is thus given by:

$$\text{anomR} = \frac{\sum_{i=1}^T (m_{\text{est},i} - \overline{m}_{\text{est}(i)}) (m_{\text{insitu},i} - \overline{m}_{\text{insitu}(i)})}{\sqrt{\sum_{i=1}^T (m_{\text{est},i} - \overline{m}_{\text{est}(i)})^2} \sqrt{\sum_{i=1}^T (m_{\text{insitu},i} - \overline{m}_{\text{insitu}(i)})^2}} \quad (35)$$

Examples of soil moisture data assimilation studies that used the anomaly correlation include *Liu et al. (2011)* and *Draper et al. (2012)*.

### 8.3 Example

Figure 5 illustrates how SMOS retrieval assimilation, using a 1D EnKF with CDF-matching, improves the ubRMSE of surface and root-zone soil moisture at select 36 km reference grid cells located in core validation watersheds across the US (Table 3). The metrics are computed using 3-hourly model output and in situ data during the period July 2010 – July 2013 at analysis time steps

only (i.e. when SMOS observations are available) and excluding frozen conditions. The dark gray bars show that the current GEOS-5 system without assimilation (open loop) performs very well, with the ubRMSE at or below  $0.04 \text{ m}^3/\text{m}^3$ . When assimilating SMOS retrievals, the ubRMSE is further reduced in both the surface and root-zone, even though the SMOS retrievals have an uncertainty at or higher than  $0.04 \text{ m}^3/\text{m}^3$ . This highlights that data assimilation has the potential to improve model results, even if the assimilated observations are very uncertain. The confidence intervals are relatively large in this example, because only 3 years of data is used at the analysis time steps only. When including forecast time steps (not shown), the reductions in ubRMSE become statistically significant.

## **9. Towards Operational Soil Moisture Data Assimilation**

A number of research and operational centers routinely generate data products that include a soil moisture analysis (in the broadest sense) at continental or global scales, either in re-analysis mode or to support operational prediction systems. Examples of data products generated with land-only systems include those from the North American Land Data Assimilation System (NLDAS, *Xia et al., 2012*) and the Global Land Data Assimilation System (GLDAS, *Rodell et al., 2004*) as well as the MERRA-Land and ERA-Land data products (section 4). These data products primarily rely on the use of precipitation observations from gauges and satellites to improve the soil moisture simulations from atmospheric assimilation systems. The NLDAS and GLDAS data products use the NASA Land Information System (LIS, *Kumar et al., 2008*) software infrastructure, which is also integrated into the atmospheric assimilation systems at the US National Oceanic and Atmospheric Administration's (NOAA) National Center for Environmental Prediction (NCEP)

1 and the US Air Force Weather Agency. At NCEP, this combined land-atmosphere assimilation  
2 system is the basis for the Climate Forecast System Reanalysis (*Saha et al., 2010*).

3  
4 The reanalysis data products benefit from the use of precipitation gauge information mainly  
5 because they are not subject to the strict latency constraints of atmospheric assimilation systems  
6 used for Numerical Weather Prediction (NWP), which require observations to be available within  
7 hours. For NWP, the objective of soil moisture data assimilation is to initialize soil moisture  
8 conditions in order to provide the best possible accuracy and consistency of surface and near-  
9 surface weather forecasts in near-real time. Operational centers such as the UK MetOffice  
10 (*Dharssi et al., 2011*), Deutscher Wetterdienst (*Hess et al., 2008*), Météo-France (*Mahfouf et al.,*  
11 *2009*), ECMWF (*de Rosnay et al., 2014*) and Environment Canada (*Bélair et al., 2003*) assimilate  
12 satellite soil moisture retrievals and/or screen level observations to update the soil moisture state.  
13 This section describes two examples of soil moisture assimilation systems: (i) the soil moisture  
14 analysis in the ECMWF Integrated Forecasting System (IFS) and (ii) the NASA Goddard Earth  
15 Observing System model, version 5 (GEOS-5) land data assimilation system used to generate a  
16 soil moisture data assimilation product for the SMAP mission.

### 17 18 *9.1 ECMWF Soil Moisture Data Assimilation for NWP*

19 The ECMWF operational soil moisture analysis relies on a point-wise “simplified EKF” approach  
20 (*de Rosnay et al., 2013*, section 6.1.1). For each grid point, the first three layers of soil moisture  
21 (of depth 0-7 cm, 7-28 cm and 28-100 cm in the ECMWF IFS) are analyzed using observations of

1 screen level temperature and relative humidity, as well as ASCAT soil moisture retrievals. In this  
2 system, the observation operator is provided by the land surface model which gives the relation  
3 between screen level temperature and humidity and soil moisture. Using screen level observations  
4 as proxy information to analyze soil moisture has proved to be very relevant for NWP applications  
5 because it consistently improves screen level variables whose accurate forecast is a key objective  
6 of NWP. However, since screen-level observations are indirectly related to soil moisture, their  
7 assimilation is effective only in areas with strong coupling between soil moisture and screen level  
8 variables. Recent developments at ECMWF focused on using satellite information from active  
9 and passive microwave sensors in addition to screen level observations, to analyze soil moisture.  
10 In particular, ASCAT soil moisture data assimilation was recently implemented in operations in  
11 May 2015.

12  
13 Figure 6 illustrates ECMWF soil moisture analysis components when screen level observations  
14 are assimilated together with ASCAT surface soil moisture data, for a six-day numerical  
15 experiment from 25 through 30 June 2013. The global NWP experiment was conducted at a  
16 resolution of 40 km as part of pre-operational tests. The soil moisture data assimilation system  
17 accounts for soil moisture background errors fixed at  $0.01 \text{ m}^3/\text{m}^3$  and observations errors of 1 K,  
18 4 % and  $0.04 \text{ m}^3/\text{m}^3$  for two meter temperature, relative humidity and ASCAT surface soil  
19 moisture, respectively. The ASCAT soil moisture index mean and range are rescaled to those of  
20 the ECMWF volumetric soil moisture using a seasonal (three month moving window) CDF-  
21 matching approach. Innovations of two meter temperature and humidity (Figure 6, c and e) indicate  
22 a good complementarity between two types of screen level observations. They generally show



warmer and/or drier conditions than the model over India and China, eastern Siberia and the northern part of South America, whereas colder and wetter conditions are observed in northern Canada, Eastern Europe and Kazakhstan. In some areas two-meter temperature and humidity innovations indicate relatively patchy discrepancies between observations and the model (e.g. Australia). There is also good agreement between ASCAT and screen level temperature and relative humidity innovations: in both cases, the observations indicate that the model is too wet over India and eastern Siberia and too dry in the eastern part of South America. Over North America, ASCAT and relative humidity innovations are also consistent in the Great Lakes area, with wetter (drier) observed conditions north (south) of the lakes. However, in Russia, ASCAT and relative humidity innovations suggest soil moisture errors of opposite sign.

The right panel of Figure 6 shows six-day accumulated increments in the first soil layer (0-7 cm) due to ASCAT data assimilation (Figure 6b), due to screen level observations assimilation (Figure 6d) and total surface soil moisture increments (Figure 6f). It shows a good complementarity between ASCAT and screen level data assimilation in term of spatial distribution of the increments. ASCAT induced increments are prominent at relatively high latitude, as well as in Argentina and Australia. Screen level data assimilation mainly contributes to soil moisture increments in Kazakhstan and North America. It is interesting to notice that there is no contribution of screen level observations to the soil moisture increments over India. This is because of rainy (monsoon) conditions that prevail at this time of the year in this region, leading to small values of the Jacobians (not shown) for screen level variables. The spatially averaged value of the combined accumulated increments is  $0.004 \text{ m}^3/\text{m}^3$  for the first soil layer, with a standard deviation

1 of 0.022 m<sup>3</sup>/m<sup>3</sup> across the map. Spatially averaged (time series) standard deviation values of 0.02  
2 m<sup>3</sup>/m<sup>3</sup> and 0.01 m<sup>3</sup>/m<sup>3</sup> are obtained for increments due ASCAT and screen level assimilation,  
3 respectively. These values indicate the average magnitude of the increments and show that the  
4 contribution of ASCAT to the top layer soil moisture increments is larger than that of screen level  
5 observations. This is consistent with the fact that satellite data provides direct information on  
6 surface soil moisture, whereas screen level observations are only indirectly related to soil moisture  
7 (but including root zone soil moisture).

8  
9 For NWP applications the assimilation window length is generally relatively short (12 hours at  
10 ECMWF). Such a time window is shorter than most of the soil diffusion processes and therefore  
11 the relation between observed surface soil moisture and root-zone soil moisture is weak. This  
12 results in low values of the Jacobian matrix elements that relate deep soil moisture to the surface  
13 soil moisture. Therefore ASCAT data assimilation mostly provides increments at surface. In the  
14 second soil layer (not shown) increments are smaller than in the first layer, with standard deviation  
15 of 0.0032 m<sup>3</sup>/m<sup>3</sup> and 0.007 m<sup>3</sup>/m<sup>3</sup> for ASCAT and screen level contributions. In the third layer  
16 most of the increments result from screen level data assimilation with negligible increments due  
17 to ASCAT data assimilation. Although the screen level observations provide only indirect  
18 information on soil moisture, their relation with root-zone soil moisture through soil-plant  
19 interaction processes makes them relevant to analyze root-zone soil moisture profile.

1 These results illustrate the complementarity between satellite information related to surface soil  
2 moisture and conventional observations related to root-zone soil moisture profiles, both in terms  
3 of spatial and vertical distributions of the increments. Future implementation plans for soil  
4 moisture data assimilation at ECMWF include the combined use of screen level observations,  
5 ASCAT soil moisture, and SMOS and SMAP brightness temperature observations.

## 6 7 *9.2 NASA SMAP Surface and Root-Zone Soil Moisture Product*

8 Global estimates of surface soil moisture estimates are routinely obtained through satellite remote  
9 sensing, but many applications need an estimate of root-zone soil moisture. The NASA SMAP  
10 mission (*Entekhabi et al., 2014*), launched on 31 January 2015, provides a number of operational  
11 soil moisture data products, including Level 2 (half-orbit) and Level 3 (daily composite) soil  
12 moisture retrievals and a value-added Level 4 Surface and Root Zone Soil Moisture (L4\_SM) data  
13 product (*Entekhabi et al., 2014, Chapter 5, p.89-100*). This latter product is based on the  
14 assimilation of SMAP 36 km brightness temperatures into the NASA GEOS-5 Catchment land  
15 surface model, using a 3D ensemble Kalman filter.

16  
17 Recall from section 4 that the model prognostic variables related to soil moisture in the Catchment  
18 land surface model are the catchment deficit (catdef), root-zone excess (rzexc), and surface excess  
19 (srfexc). Other relevant model prognostic variables are the land surface temperature (tsurf) and  
20 the near-surface ground heat content (ght) which determines the near-surface soil temperature  
21 (tsoil). These soil moisture variables as well as the forcings are suitably perturbed to generate an  
22 ensemble of forecasts (Table 2, section 7.2.1). A radiative transfer model (section 5.2) diagnoses

brightness temperature based on the surface soil moisture and temperature in the assimilation system, i.e.  $\widehat{Tb_{i,j}} = h(\widehat{x_{i,j}})$  for each time step  $i$  and ensemble member  $j$ . This radiative transfer model is optimized to simulate a realistic long-term mean and variability in brightness temperature. The optimization is based on multi-angular SMOS observations and uses statistically optimized estimates of simulation and observation errors (*De Lannoy et al., 2013*). Consequently, long-term biases between observations and observation predictions  $[Tb_{obs,i,j} - \widehat{Tb_{i,j}}]$  are small by design but seasonal biases are still present. To deal with the remaining biases, the instantaneous  $Tb_{obs,i}$  are rescaled to the model climatology using seasonally varying means, as discussed in section 7.1.1 (Figure 3b). The data assimilation then maps the differences between the rescaled brightness temperature observations and simulations to increments in the prognostic variables of the Catchment land surface model.

Figure 7 illustrates the concept of assimilating coarse-scale ( $\sim 36$  km) brightness temperatures into the GEOS-5 Catchment land surface model. In the absence of SMAP observations at the time of writing, SMOS (*Kerr et al., 2010*) brightness temperature observations are assimilated at  $40^\circ$  incidence angle, for both H- and V-polarization. For simplicity, it is assumed here that the state variables and observations are at the same coarse-scale 36 km resolution. Note however that the SMAP L4\_SM product is produced at 9 km.

Figures 7a-b show the ensemble mean innovations  $\langle Tb'_{obs,i} - \widehat{Tb_i} \rangle$  for (a) horizontal polarization and (b) vertical polarization and for both ascending and descending overpasses during 3 days. The swaths are relatively narrow, because of the strict quality control against aliased data and quality control on the angular fitting from multi-angular data to  $40^\circ$  incidence brightness temperature.

1 Some swaths are also incomplete because insufficient historical data are available (often due to  
2 radiofrequency interference, primarily over China, the Middle East, and Eastern Europe) to ensure  
3 a statistically reliable rescaling.

4  
5 Figures 7c-f illustrate how the brightness temperature innovations are mapped to state increments.  
6 Negative brightness temperature innovations in Figures 7a-b indicate that the model is too warm  
7 and/or too dry. Consequently, the negative innovations in the central western region of the US  
8 and in the southwestern region of Australia result in an increase in soil moisture and a decrease  
9 the soil temperature. Likewise, positive innovations result in a decrease in soil moisture and an  
10 increase in soil temperature. Note that an increase in soil moisture corresponds to an increase in  
11 the water excess terms (srfexc, rzexc) and a decrease in the water deficit term (catdef). The  
12 magnitude of the increments to srfexc, rzexc and catdef should be interpreted in relation to the  
13 storage capacity of each of these components (with equivalent soil layer thicknesses of 0.05 m, 1  
14 m, 1.3-10 m, respectively) and the colorbar range is scaled accordingly. While the absolute values  
15 of the increments are largest for catdef (global standard deviation of about 5 mm, pertaining to the  
16 entire profile), the increments relative to the layer depth are largest in the 5 cm surface layer  
17 (srfexc).

18  
19 The spatial filtering introduces some additional important features: the increments are spatially  
20 smoothed and the spatial coverage of the increments is wider than the coverage of brightness  
21 temperature innovations. The spatial error correlations also introduce a horizontal propagation of  
22 information to unobserved areas. In this example, the support of the forecast error correlation

function is limited to  $1.25^\circ$  and increments thus taper off over a distance of  $1.25^\circ$  away from the observed swath. The L4\_SM product is generated on a 9 km model grid and the spatial filtering further improves soil moisture estimation through downscaling of 36 km brightness temperature innovations.

The L4\_SM product is not limited to global surface and root-zone soil moisture. Research output includes other land surface state variables such as soil temperature and snow, as well as land surface fluxes and meteorological forcings. In addition, ensemble-derived error estimates are provided.

## **10. Summary**

Soil moisture is a key variable in hydrological and Earth modeling and assimilation systems. Good estimates of soil moisture at regional to global scales are important for predictions of weather and climate, agricultural productivity, natural hazards and for various other environmental and socio-economic applications. Data assimilation provides a means to obtain enhanced soil moisture estimates by combining (often indirect) observations of soil moisture with land surface modeling. At large spatial scales, observations related to soil moisture are mainly provided by global surface observational networks or through remote sensing, either in the form of satellite retrievals, microwave radiances or backscatter values. This chapter provides conceptual examples on how to assimilate these observations with widely accepted assimilation techniques, such as optimal interpolation and various types of Kalman filtering and smoothing. Special attention is paid to

1 practical issues, such as dealing with multiple scales, the treatment of typical biases and the  
2 characterization of random forecast and observation errors.

3  
4 Operational centers have used screen-level observations of temperature and relative humidity to  
5 update soil moisture and temperature for numerical weather prediction. Satellite-based microwave  
6 observations provide more direct measurements of surface soil moisture and recent satellite  
7 missions such as ASCAT, SMOS and SMAP are aiming at continued and improved surface soil  
8 moisture observations. The assimilation of satellite-based surface soil moisture retrievals has the  
9 capability to improve both surface and root-zone soil moisture, as illustrated in various research  
10 applications. However, the soil moisture retrieval process relies on parameters and a priori  
11 information that may be inconsistent with the land surface model used in the assimilation system.  
12 It is thus more natural to couple a radiative transfer or backscatter model to a land surface model,  
13 and then directly assimilate microwave observations such as brightness temperature or backscatter.  
14 Further improvements in continental-scale root-zone soil moisture can perhaps be obtained from  
15 the assimilation of integrated terrestrial water storage observations (e.g. from GRACE).

16  
17 The growing experience with assimilation of soil moisture observations is reflected in the  
18 preparation of new cutting-edge data assimilation systems for operational applications. This  
19 chapter provides details on two of these systems. A first example shows how ASCAT surface soil  
20 moisture retrievals will be assimilated along with screen-level observations for numerical weather  
21 prediction at ECMWF. A second example discusses the assimilation of brightness temperature

1 observations from SMOS to prepare for the operational global SMAP surface and root-zone  
2 product (L4\_SM) at NASA. Both these systems benefit from increasingly available computational  
3 power as well as from recent and future satellite missions that are specifically designed to measure  
4 soil moisture. These operational systems are able to provide improved soil moisture estimates that  
5 have the potential to improve hydro-meteorological forecasting across a range of applications such  
6 as weather forecasting and the monitoring and prediction of droughts.

## 9 **Acknowledgment**

10 Gabriëlle De Lannoy and Rolf Reichle were supported by the NASA Soil Moisture Active Passive  
11 mission (SMAP). The authors thank Clara Draper and Qing Liu for helpful discussions, and Hans  
12 Lievens for his help with the Integral Equation Model. In situ soil moisture observations are  
13 provided by Michael Cosh and Tom Jackson from USDA (core validation data for SMAP).



## References

1. Albergel C, Dorigo W, Reichle R, Balsamo G, de Rosnay P, Muñoz-Sabater J, Isaksen L, de Jeu R, Wagner W (2013). Skill and global trend analysis of soil moisture from reanalyses and microwave remote sensing. *Journal of Hydrometeorology*, 14: 1259-1277. doi: 10.1175/JHM-D-12-0161.1.
2. Balsamo G, Albergel C, Beljaars A, Boussetta S, Cloke H, Dee D, Dutra E, Muñoz-Sabater J, Pappenberger F, de Rosnay P, Stockdale T, Vitart F (2013). ERA-Interim/Land: a global land water resources dataset. *HESS*, 10:14705-14745. doi:10.5194/hessd-10-14705-2013.
3. Balsamo G, Viterbo P, Beljaars A, van den Hurk B, Hirschi M, Betts AK, Scipal K (2009). A revised hydrology for the ECMWF model: Verification from field site to terrestrial water storage and impact in the integrated forecast system. *Journal of Hydrometeorology*, 10:623-643. doi: 10.1175/2008JHM1068.1.
4. Balsamo G, Mahfouf JF, Bélair S, Deblonde G (2006). A global root-zone soil moisture analysis using simulated L-band brightness temperature in preparation for the Hydros satellite mission. *Journal of Hydrometeorology*, 7: 1126–1146.
5. Bélair S, Crevier LP, Mailhot J, Bilodeau B, Delage Y (2003). Operational implementation of the ISBA land surface scheme in the Canadian regional weather forecast model. Part I: Warm season results. *Journal of Hydrometeorology*, 4: 352–370.
6. Bartalis Z, Wagner W, Naeimi V, Hasenauer S, Scipal K, Bonekamp H, Figa J, Anderson. (2007). Initial soil moisture retrievals from the METOP-A Advanced Scatterometer (ASCAT). *Geophysical Research Letters*, 34: L20401. doi:10.1029/2007GL031088.
7. Crow WT, Yilmaz MT (2014). The Auto-Tuned Land Data Assimilation System (ATLAS). *Water Resources Research*, 50: 371–385. doi:10.1002/2013WR014550.
8. De Lannoy GJM, Houser PR, Pauwels VRN, Verhoest NE. (2006). Assessment of model uncertainty for soil moisture through ensemble verification. *Journal of Geophysical Research*, 111:D10101, doi:10.1029/2005JD006367.
9. De Lannoy G, Reichle R, Pauwels V (2013). Global calibration of the GEOS-5 L-band microwave radiative transfer model over non-frozen land using SMOS observations. *Journal of Hydrometeorology*, 14: 765–785. doi: 10.1175/JHM-D-12-092.1.
10. De Lannoy GJM, Reichle RH, Houser PR, Pauwels VRN, Verhoest NEC (2007). Correcting for forecast bias in soil moisture assimilation with the ensemble Kalman filter. *Water Resources Research*, 43, W09410. doi:10.1029/2006WR00544.
11. de Rosnay P, Drusch M, Vasiljevic D, Balsamo G, Albergel C, Isaksen L (2013). A simplified Extended Kalman Filter for the global operational soil moisture analysis at ECMWF. *Q. J. R. Meteorol. Soc.*, 139(674):1199-1213. doi: 10.1002/qj.2023.
12. de Rosnay P, Balsamo G, Albergel C, Muñoz-Sabater J, Isaksen . (2014). Initialisation of land surface variables for Numerical Weather Prediction. *Surveys in Geophysics*, 35(3): 607-621. doi: 10.1007/s10712-012-9207-x.
13. Dharssi I, Bovis KJ, Macpherson B, Jones CP (2011). Operational assimilation of ASCAT surface soil wetness at the Met Office. *HESS*, 15: 2729–2746. doi:10.5194/hess-15-2729-2011.
14. Dirmeyer P (2000). Using a global soil wetness dataset to improve seasonal climate simulation. *Journal of Climate*, 13:2900–2921.

- 1 15. Dorigo WA, Gruber A, de Jeu RAM, Wagner W, Stacke T, Loew A, Albergel C, Brocca  
2 L, Chung D, Parinussa R, Kidd R (2015). Evaluation of the ESA CCI soil moisture product  
3 using groundbased observations, *Remote Sensing of Environment*, 162, 380–395,  
4 doi:10.1016/j.rse.2014.07.023.
- 5 16. Draper CS, Reichle RH, De Lannoy GJM, Liu Q (2012). Assimilation of passive and active  
6 microwave soil moisture retrievals. *Geophysical Research Letters*, 39: L04401.  
7 doi:10.1029/2011GL050655.
- 8 17. Drusch M, Scipal K, de Rosnay P, Balsamo G, Andersson E, Bougeault P, Viterbo P  
9 (2009). Towards a Kalman Filter-based soil moisture analysis system for the operational  
10 ECMWF Integrated Forecast System. *Geophysical Research Letters*, 36: L10401. doi:  
11 10.1029/2009GL037716.
- 12 18. Drusch M, Wood EF, Gao H (2005). Observation operators for the direct assimilation of  
13 TRMM microwave imager retrieved soil moisture. *Geophysical Research Letters*, 32:  
14 L15403. doi:10.1029/2005GL023623.
- 15 19. Dunne S, Entekhabi D (2006). Land surface state and flux estimation using the ensemble  
16 Kalman smoother during the Southern Great Plains 1997 field experiment. *Water*  
17 *Resources Research*, 42: W01407.
- 18 20. Entekhabi D, Nakamura H, Njoku EG (1994). Solving the inverse problems for soil  
19 moisture and temperature profiles by sequential assimilation of multifrequency remotely-  
20 sensed observations. *IEEE Transactions in Geoscience and Remote Sensing*, 32: 438-448.
- 21 21. Entekhabi D., Reichle RH, Koster RD, Crow WT (2010). Performance Metrics for Soil  
22 Moisture Retrievals and Application Requirements. *Journal of Hydrometeorology*, 11:  
23 832-840. doi:10.1175/2010JHM1223.1.
- 24 22. Entekhabi D, and Coauthors (2014). The SMAP Handbook. NASA/JPL, 183p, in press.
- 25 23. Fung AK, Li Z, Chen KS (1992). Backscattering from a randomly rough dielectric surface.  
26 *IEEE Transactions in Geoscience and Remote Sensing*, 30: 356–369.
- 27 24. Giard D, Bazile E (2000). Implementation of a new assimilation scheme for soil and  
28 surface variables in a global NWP model. *Monthly Weather Review*, 128: 997-1015.
- 29 25. Gleick PH (1996). Water resources. In *Encyclopedia of Climate and Weather*, ed. by S. H.  
30 Schneider, Oxford University Press, New York, 2:817-823.
- 31 26. Hess R, Lange M, Werner W (2008). Evaluation of the variational soil moisture  
32 assimilation scheme at Deutscher Wetterdienst. *HESS*, 134(635): 1499-1512.
- 33 27. Kerr Y, and Coauthors (2010). The SMOS mission: New tool for monitoring key elements  
34 of the global water cycle. *Proceedings of the IEEE*, 98: 666-687.
- 35 28. Koster RD, Dirmeyer PA, Guo Z, Bonan G, Cox P, Gordon C, Kanae S, Kowalczyk E,  
36 Lawrence D, Liu P, Lu C, Malyshev S, McAvaney B, Mitchell K, Mocko D, Oki T, Oleson  
37 K, Pitman A, Sud Y, Taylor C, Versegny D, Vasic R, Xue Y, Yamada T (2004) Regions  
38 of strong coupling between soil moisture and precipitation. *Science* 305:1138–1140.
- 39 29. Koster RD, Suarez MJ, Ducharne A, Stieglitz M, Kumar P (2000). A catchment-based  
40 approach to modeling land surface processes in a general circulation model 1. Model  
41 structure. *Journal of Geophysical Research*, 105 (D20): 24 809–24 822.
- 42 30. Kumar S, Peters-Lidard C, Tian Y, Reichle R, Geiger J, Alonge C, Eylander J, Houser P  
43 (2008). An integrated hydrologic modeling and data assimilation framework, *IEEE*  
44 *Computer*, 41: 52-59. doi:10.1109/MC.2008.511.

31. Liu Q, Reichle RH, Bindlish R, Cosh MH, Crow WT, de Jeu R, De Lannoy GJM, Huffman GJ, Jackson TJ (2011). The contributions of precipitation and soil moisture observations to the skill of soil moisture estimates in a land data assimilation system, *Journal of Hydrometeorology*, 12: 750-765. doi:10.1175/JHM-D-10-05000.
32. Mahfouf JF, Bergaoui K, Draper C, Bouysse F, Taillefer F, Taseva L (2009), A comparison of two off-line soil analysis schemes for assimilation of screen level observations. *Journal of Geophysical Research*, 114: D08105. doi:10.1029/2008JD011077.
33. Mo T, Choudhury BJ, Schmugge TJ, Wang JR, Jackson TJ (1982). A model for microwave emission from vegetation-covered fields. *Journal of Geophysical Research Oceans Atmos.*, 87(C13): 1229–1237.
34. Montzka C, Grant JP, Moradkhani J, Hendricks-Franssen HJ, Weihermüller L., Drusch M., Vereecken H (2013). Estimation of radiative transfer parameters from L-Band passive microwave brightness temperatures using advanced data assimilation, *Vadose Zone Journal*, 12(3), doi:10.2136/vzj2012.0040.
35. Pan M, Wood EF, Wojcik R, McCabe MF (2008). Estimation of regional terrestrial water cycle using multi-sensor remote sensing observations and data assimilation. *Remote Sensing of Environment*, 112: 1282–1294.
36. Pauwels VRN, De Lannoy GJM (2009). Ensemble-based assimilation of discharge into rainfall-runoff models: a comparison of approaches to mapping observational information to state space. *Water Resources Research*, 45(8): W08428. doi:10.1029/2008WR007590.
37. Reichle RH, De Lannoy GJM, Forman BA, Draper CS, Liu Q (2014). Connecting satellite observations with water cycle variables through land data assimilation: Examples using the NASA GEOS-5 LDAS. *Surveys of Geophysics*, 35: 577-606. doi:10.1007/s10712-013-9220-8.
38. Reichle RH, Entekhabi D, McLaughlin D (2001). Downscaling of radio brightness measurements for soil moisture estimation: A four dimensional variational data assimilation approach. *Water Resources Research*, 37: 2353–2364.
39. Reichle RH, Koster RD (2004). Bias reduction in short records of satellite soil moisture. *Geophysical Research Letters*, 31: L19501. doi:10.1029/2004GL020938.
40. Reichle RH, Koster RD (2003). Assessing the impact of horizontal error correlations in background fields on soil moisture estimation. *Journal of Hydrometeorology*, 4 (6): 1229-1242.
41. Reichle RH, Koster RD, De Lannoy GJM, Forman BA, Liu Q, Mahanama SPP, Toure A (2011). Assessment and enhancement of MERRA land surface hydrology estimates. *Journal of Climate*, 24: 6322–6338.
42. Reichle RH, McLaughlin DB, Entekhabi D. (2002). Hydrologic data assimilation with the ensemble Kalman filter. *Monthly Weather Review*, 120:103–114.
43. Rodell M, Chen J, Kato H, Famiglietti JS, Nigro J, Wilson CR (2007). Estimating ground water storage changes in the Mississippi River basin (USA) using GRACE. *Hydrogeology Journal*, 15: 159-166.
44. Rodell M, Houser PR, Jambor U, Gottschalck J, Mitchell K, Meng CJ, Arsenault K, Cosgrove B, Radakovich J, Bosilovich M, Entin JK, Walker JP, Lohmann D, Toll D (2004). The Global Land Data Assimilation System. *Bulletin of the American Meteorological Society*, 85(3): 381-394.

- 1 45. Sabater, J, Jarlan, L, Calvet J, Bouyssel F, de Rosnay P (2007). From near-surface to root-  
2 zone soil moisture using different assimilation techniques. *Journal of Hydrometeorology*,  
3 8(2): 194–206
- 4 46. Saha S, and Co-authors (2010). The NCEP Climate Forecast System Reanalysis. *Bulletin*  
5 *of the American Meteorological Society*, doi:10.1175/2010Bams3001.1
- 6 47. Scipal K, Holmes T, de Jeu R, Naeimi V, Wagner W (2008). A possible solution for the  
7 problem of estimating the error structure of global soil moisture data sets. *Geophysical*  
8 *Research Letters*, 35: L24403.1-4.
- 9 48. Wigneron JP, and Coauthors (2007). L-band microwave emission of the biosphere (L-  
10 MEB) model: Description and calibration against experimental data sets over crop fields.  
11 *Remote Sensing of Environment*, 107: 639–655.
- 12 49. Xia Y, Mitchell K, Ek M, Sheffield J, Cosgrove B, Wood E, Luo L, Alonge C, Wei H,  
13 Meng J, Livneh B, Lettenmaier D, Koren V, Duan Q, Mo K, Fan Y, Mocko D (2012).  
14 Continental scale water and energy flux analysis and validation for the North American  
15 Land Data Assimilation System project phase 2 (NLDAS-2): 1. Intercomparison and  
16 application of model products. *Journal of Geophysical Research*, 117: D03109.  
17 doi:10.1029/2011JD016048.
- 18 50. Zaitchik BF, Rodell M, Reichle RH (2008). Assimilation of GRACE terrestrial water  
19 storage data into a land surface model: results for the Mississippi river basin. *Journal of*  
20 *Hydrometeorology*, 9:535–548.
- 21

1 **Table 1:** Summary of (1) forecast and (2) update equations for optimal interpolation (OI),  
2 (Extended) Kalman filtering ((E)KF) and ensemble Kalman filtering (EnKF). The OI and (E)KF  
3 use a single state trajectory and a predefined or linearly evolving  $\mathbf{P}_i^-$ , respectively, whereas the  
4 EnKF uses N ensemble members, perturbed with model error  $\mathbf{w}_{i,j}$  to diagnose  $\mathbf{P}_i^-$ .

OI, (E)KF	EnKF
<b>(1) A priori state and uncertainty</b>	
$\hat{\mathbf{x}}_i^- = f_{i,i-1}(\hat{\mathbf{x}}_{i-1}^+, \mathbf{u}_i, \boldsymbol{\alpha})$	$\hat{\mathbf{x}}_{i,j}^- = f_{i,i-1}(\hat{\mathbf{x}}_{i-1,j}^+, \mathbf{u}_i, \boldsymbol{\alpha}, \mathbf{w}_{i,j})$ with $j=1, \dots, N$
$\mathbf{P}_i^- = \mathbf{B}$ (OI)	$\mathbf{P}_i^- = \text{Cov}(\hat{\mathbf{x}}_i^-, \hat{\mathbf{x}}_i^-)$
$\mathbf{P}_i^- = \mathbf{F}_{i,i-1} \mathbf{P}_{i-1}^+ \mathbf{F}_{i,i-1}^T + \mathbf{Q}_i$ (EKF)	
Observation predictions	
$\hat{\mathbf{y}}_i^- = \mathbf{h}_i(\hat{\mathbf{x}}_i^-, \boldsymbol{\beta})$	$\hat{\mathbf{y}}_{i,j}^- = \mathbf{h}_i(\hat{\mathbf{x}}_{i,j}^-, \boldsymbol{\beta})$
<b>(2) A posteriori state and uncertainty</b>	
$\mathbf{K}_i = \mathbf{P}_i^- \mathbf{H}_i^T [\mathbf{H} \mathbf{P}_i^- \mathbf{H}^T + \mathbf{R}]_i^{-1}$	$\mathbf{K}_i = \text{Cov}(\hat{\mathbf{x}}_i^-, \hat{\mathbf{y}}_i^-) [\text{Cov}(\hat{\mathbf{y}}_i^-, \hat{\mathbf{y}}_i^-) + \mathbf{R}_i]^{-1}$
$\hat{\mathbf{x}}_i^+ = \hat{\mathbf{x}}_i^- + \mathbf{K}_i [\mathbf{y}_{\text{obs},i} - \hat{\mathbf{y}}_i^-]$	$\hat{\mathbf{x}}_{i,j}^+ = \hat{\mathbf{x}}_{i,j}^- + \mathbf{K}_i [\mathbf{y}_{\text{obs},i,j} - \hat{\mathbf{y}}_{i,j}^-]$ $\hat{\mathbf{x}}_i^+ = \frac{1}{N} \sum_{j=1}^N \hat{\mathbf{x}}_{i,j}^+$
$\mathbf{P}_i^+ = [\mathbf{I} - \mathbf{K} \mathbf{H}]_i \mathbf{P}_i^-$	$\mathbf{P}_i^+ = \text{Cov}(\hat{\mathbf{x}}_i^+, \hat{\mathbf{x}}_i^+)$

5

- 1 **Table 2:** Example of perturbations to forcing and model prognostic variable in the GEOS-5 land  
2 data assimilation system for brightness temperature assimilation. Values are from the preliminary  
3 system calibration used for the results discussed in section 9.2.

Perturbation	Additive (A) or Multipli- cative (M)	Standard deviation	AR(1) time series correla- tion scale	Spatial correla- tion scale	Cross-correlation with perturbations in		
					P	SW	LW
Precipitation (P)	M	0.5	24 h	50 km	n/a	-0.8	0.5
Downward shortwave (SW)	M	0.3	24 h	50 km	-0.8	n/a	-0.5
Downward longwave (LW)	A	20 W/m <sup>2</sup>	24 h	50 km	0.5	-0.5	n/a
					catdef	srfexc	
Catchment deficit (catdef)	A	0.24 kg/m <sup>2</sup> /h	3 h	50 km	n/a	0.0	
Surface excess (srfexc)	A	0.16 kg/m <sup>2</sup> /h	3 h	50 km	0.0	n/a	

4

5

1 **Table 3:** Details of core validation sites (*Entekhabi et al., 2014*) and 36 km reference grid cells  
2 within each site used for independent validation of the SMOS data assimilation experiment in  
3 section 8.3. Each reference grid cell contains a minimum of 5 sensors and a maximum of N sensors.  
4 The latitude and longitude refer to the center of 36 km grid cells on the Equal-Area Scalable Earth  
5 Grid version 2.

Core site	State (US)	Reference grid cell	Latitude (°N)	Longitude (°W)	Maximum N sensors
Reynolds Creek	Idaho	RC1	43.33	116.70	6
		RC2	42.95	116.70	9
Walnut Gulch	Arizona	WG1	31.96	110.73	6
		WG2	31.62	110.35	14
		WG3	31.62	109.98	22
Little Washita	Oklahoma	LW	34.99	98.03	15
Fort Cobb	Oklahoma	FC	35.34	98.40	10
Little River	Georgia	LR1	31.62	83.84	15
		LR2	31.62	83.46	12
Saint Joseph	Indiana	SJ	41.43	84.96	15
South Fork	Iowa	SF	42.57	93.55	12

6

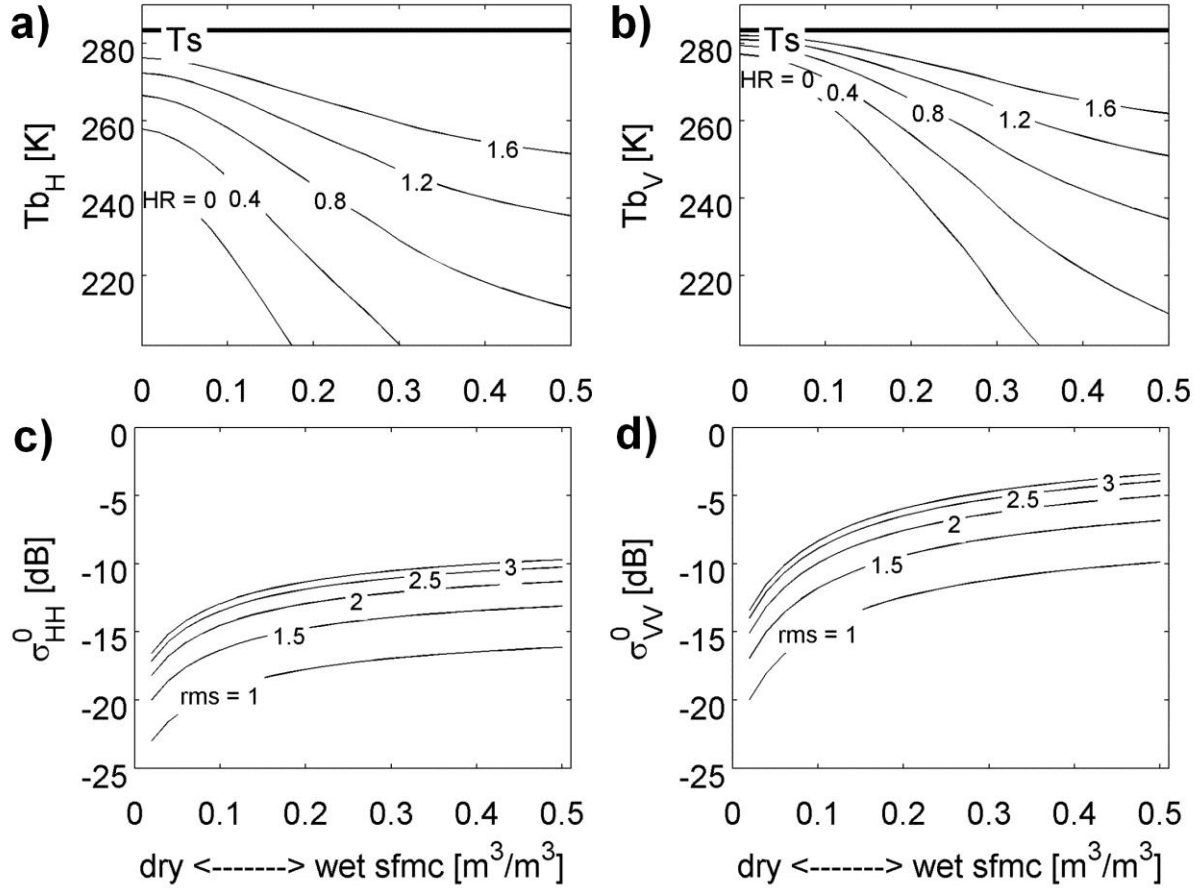


**Figure 1:** (Top) Relationship between soil moisture (sfmc) and brightness temperature ( $T_b$ ) at (a) horizontal and (b) vertical polarization. (Bottom) Same but for radar backscatter ( $\sigma^0$ ) at (c) horizontal and (d) vertical co-polarization. The soil contains 43% sand, 23% clay and has a bulk density of  $1.24 \text{ g/cm}^3$ . The weighted surface/soil temperature ( $T_s$ ) is set to 283 K. The sensor-specific constants are following the SMAP instrument details ( $40^\circ$  incidence angle, radar at 1.29 GHz, radiometer at 1.41 GHz).



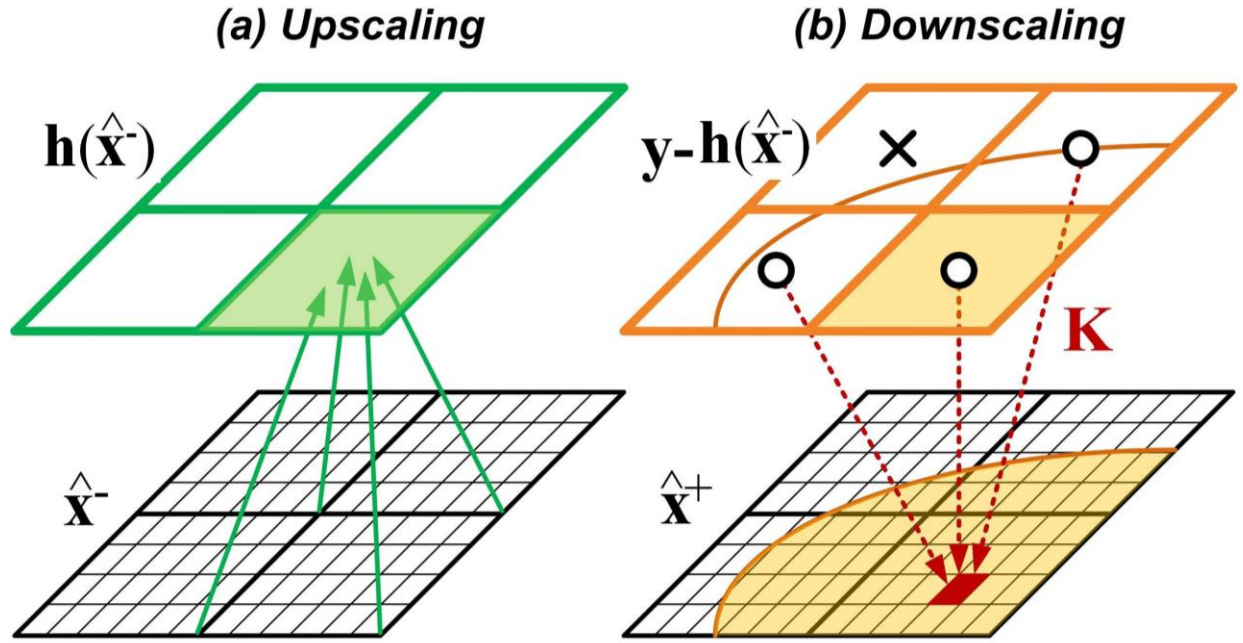


**Figure 2:** Schematic of a multi-scale 3D filter. (a) State variables in fine-scale model gridcells are aggregated to coarse-scale observation predictions through the observation operator  $\mathbf{h}(\cdot)$ . (b) Coarse-scale innovations (observation-minus-forecasts,  $\mathbf{y}_{\text{obs},i} - \mathbf{h}(\hat{\mathbf{x}}_i^-)$ ) located within the influence radius (curved shaded area) around a fine-scale model grid cell are indicated by circles and will contribute to the fine-scale state update.

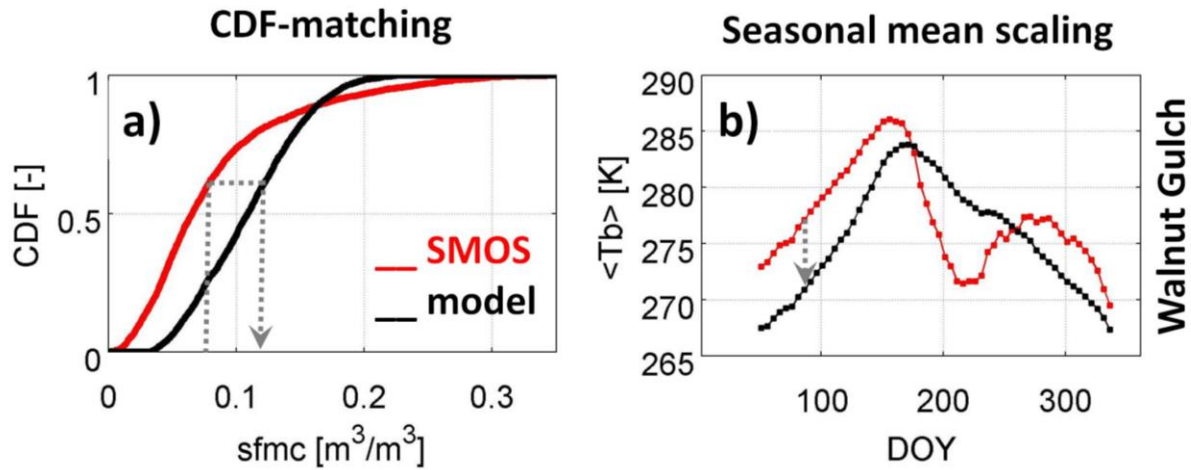


**Figure 3:** Illustration of scaling techniques to remove bias from the innovations in the assimilation soil moisture observations at a single 36 km grid cell in Walnut Gulch (WG3, see Table 3). (a) CDFs of soil moisture from SMOS retrievals and GEOS-5 simulations. (b) Seasonal climatology of SMOS-observed and simulated brightness temperatures (horizontal polarization, 40° incidence angle, ascending overpass, smoothed and multi-year averaged). Both figures are based on 3 years (1 July 2010 – 1 July 2013) of data.

**Ratio of analysis to forecast ensemble std-dev in sfmc**  
**spatial m = 0.81, s = 0.13 [-]**

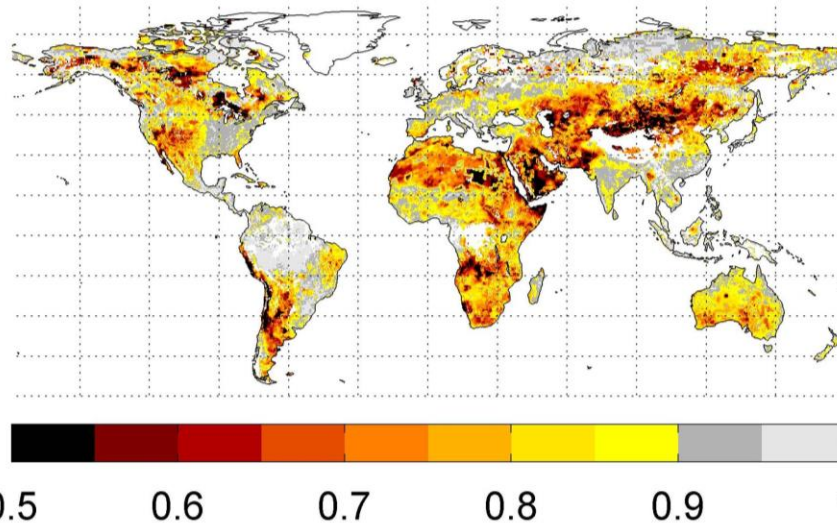


**Figure 4:** Ratio of the analysis error standard-deviation (std-dev) to the forecast ensemble standard deviation in surface soil moisture averaged over 3 years (July 2010-July 2013). The analysis is obtained by assimilating both ascending and descending SMOS soil moisture retrievals (v551) in the GEOS-5 land data assimilation system. Locations with less than 50 SMOS retrievals available for assimilation are shown in white. The spatial mean and standard deviation are denoted by m and s in the figure title.

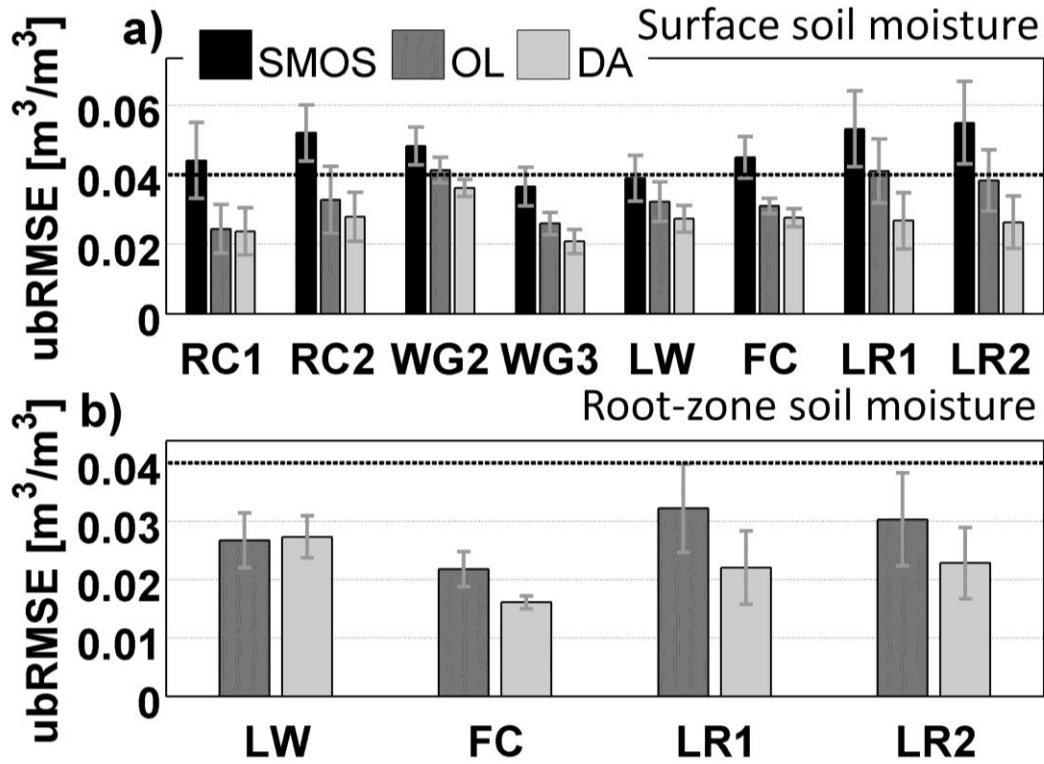


**Figure 5:** Performance of (a) surface and (b) root-zone soil moisture in terms of ubRMSE for (black) both ascending and descending SMOS retrievals, (dark gray) open loop, and (light gray) SMOS retrieval data assimilation at various 36 km core validation sites across the US (Table 3). The metrics are based on 3 years (1 July 2010-1 July 2013) of 3-hourly output at the analysis time steps only. The error bars indicate the 99% confidence intervals.

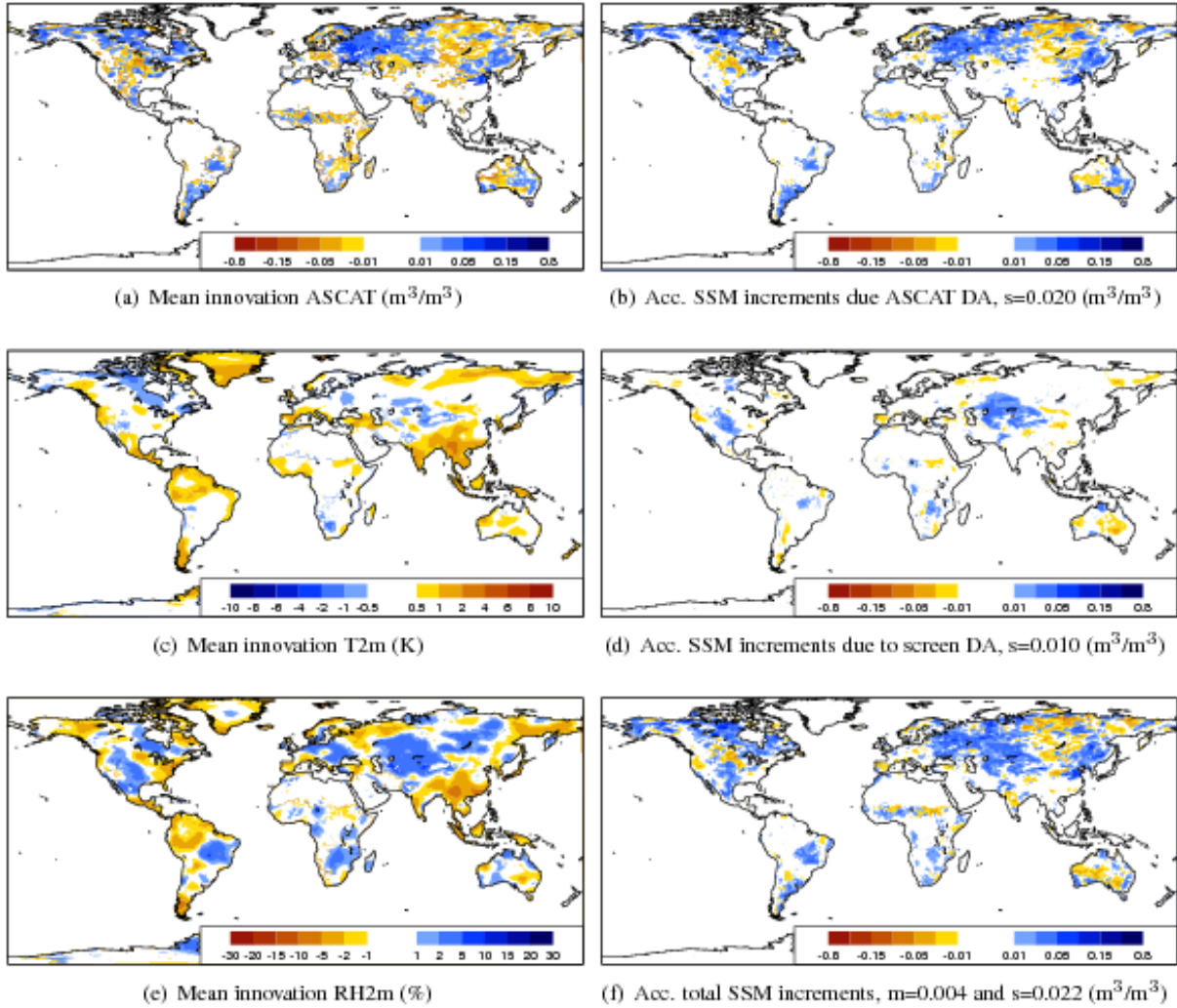


**Figure 6:** Illustration of ECMWF soil moisture analysis (left) mean innovations and (right) accumulated soil moisture increments for a six-day period from 25 through 30 June 2013. Innovations show the differences between observations and ECMWF first guess for (a) scaled ASCAT observations and ECMWF surface soil moisture (in  $\text{m}^3/\text{m}^3$ ), (c) two-meter temperature (K) and (e) two-meter relative humidity (%). Right panel shows accumulated surface soil moisture increments ( $\text{m}^3/\text{m}^3$ ) due to (b) ASCAT data assimilation, (d) screen level data assimilation and (f) total accumulated increments. The spatial mean and standard deviation are denoted by  $m$  and  $s$  in the figure titles.

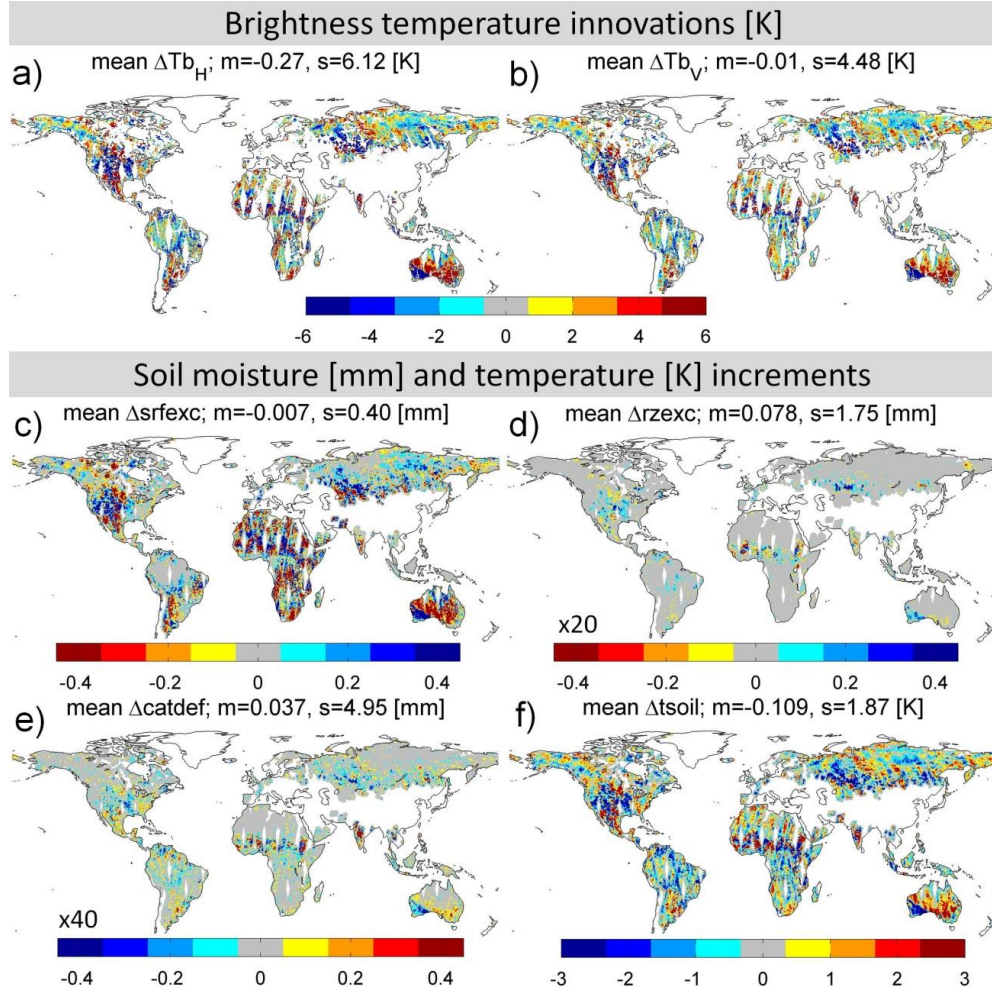


**Figure 7:** (Top) illustration of differences between scaled SMOS-observed and NASA GEOS-5 simulated brightness temperatures at  $40^\circ$  incidence angle for (a) H- and (b) V-polarization. (Bottom) temporally averaged increments ( $\Delta$ ) to the Catchment land surface model (c) srfexc, (d) rzexc and (e) catdef and (f) tsoil, after assimilation of SMOS brightness temperatures. The range of the colorbars for rzexc is 20 times that of the srfexc, because rzexc applies to a 1 m root-zone, while srfexc applies to a 0.05 m surface layer. For catdef, the colorbar scaling factor of 40 is motivated by the average depth of bedrock (or profile soil moisture layer thickness) of 2 m. The time period covers ascending and descending orbits for a 3 days from 27 through 29 July 2013. The spatial mean and standard deviation are denoted by m and s in the figure titles.